



HAL
open science

Cell redistribution of G quadruplex-structured DNA is associated with morphological changes of nuclei and nucleoli in neurons during tau pathology progression

Thomas Comptdaer, Meryem Tardivel, Claire Schirmer, Luc Buee,
Marie-Christine Galas

► To cite this version:

Thomas Comptdaer, Meryem Tardivel, Claire Schirmer, Luc Buee, Marie-Christine Galas. Cell redistribution of G quadruplex-structured DNA is associated with morphological changes of nuclei and nucleoli in neurons during tau pathology progression. *Brain Pathology*, 2024, *Brain Pathology*, pp.e13262. 10.1111/bpa.13262 . hal-04685000

HAL Id: hal-04685000

<https://hal.univ-lille.fr/hal-04685000v1>

Submitted on 3 Sep 2024

HAL is a multi-disciplinary open access archive for the deposit and dissemination of scientific research documents, whether they are published or not. The documents may come from teaching and research institutions in France or abroad, or from public or private research centers.

L'archive ouverte pluridisciplinaire **HAL**, est destinée au dépôt et à la diffusion de documents scientifiques de niveau recherche, publiés ou non, émanant des établissements d'enseignement et de recherche français ou étrangers, des laboratoires publics ou privés.



Distributed under a Creative Commons Attribution - NonCommercial - NoDerivatives 4.0 International License

RESEARCH ARTICLE

Cell redistribution of G quadruplex-structured DNA is associated with morphological changes of nuclei and nucleoli in neurons during tau pathology progression

Thomas Comptdaer¹ | Meryem Tardivel² | Claire Schirmer¹ | Luc Buée¹ | Marie-Christine Galas¹ 

¹University of Lille, Inserm, CHU Lille, CNRS, LiNCog-Lille Neuroscience and Cognition, Lille, France

²University of Lille, CNRS, Inserm, CHU Lille, Institut Pasteur de Lille, US41-UAR 2014-PLBS, Lille, France

Correspondence

Marie-Christine Galas, University of Lille, Inserm, CHU Lille, CNRS, LiNCog-Lille Neuroscience and Cognition, F-59000 Lille, France.

Email: marie-christine.galas@inserm.fr

Present address

Claire Schirmer, Eidgenössische Technische Hochschule Zürich, Zurich, Switzerland.

Funding information

Investissement d'avenir LabEx (Laboratory Excellence) DISTALZ (Development of Innovative Strategies for a Transdisciplinary approach to Alzheimer's disease); EU Joint Programme - Neurodegenerative Disease Research (JPND), Grant/Award Number: INSTALZ_643417; LICEND (Lille Centre of Excellence for Neurodegenerative Disorders); CNRS (Centre National de la Recherche Scientifique); Inserm (Institut National de la Santé et de la Recherche Médicale); Métropole Européenne de Lille; University of Lille; FEDER; Research Foundation Flanders; Innovation Fund Denmark; Agence Nationale de la Recherche; Swedish Research Council; Medical Research Council; European Union's Horizon 2020 research and innovation programme

Abstract

While the double helical structure has long been its iconic representation, DNA is structurally dynamic and can adopt alternative secondary configurations. Specifically, guanine-rich DNA sequences can fold in guanine quadruplexes (G4) structures. These G4 play pivotal roles as regulators of gene expression and genomic stability, and influence protein homeostasis. Despite their significance, the association of G4 with neurodegenerative diseases such as Alzheimer's disease (AD) has been underappreciated. Recent findings have identified DNA sequences predicted to form G4 in sarkosyl-insoluble aggregates from AD brains, questioning the involvement of G4-structured DNA (G4 DNA) in the pathology. Using immunofluorescence coupled to confocal microscopy analysis we investigated the impact of tau pathology, a hallmark of tauopathies including AD, on the distribution of G4 DNA in murine neurons and its relevance to AD brains. In healthy neurons, G4 DNA is detected in nuclei with a notable presence in nucleoli. However, in a transgenic mouse model of tau pathology (THY-Tau22), early stages of the disease exhibit an impairment in the nuclear distribution of G4 DNA. In addition, G4 DNA accumulates in the cytoplasm of neurons exhibiting oligomerized tau and oxidative DNA damage. This altered distribution persists in the later stage of the pathology when larger tau aggregates are present. Still cytoplasmic deposition of G4 DNA does not appear to be a critical factor in the tau aggregation process. Similar patterns are observed in neurons from the AD cortex. Furthermore, the disturbance in G4 DNA distribution is associated with various changes in the size of neuronal nuclei and nucleoli, indicative of responses to stress and the activation of pro-survival mechanisms. Our results shed light on a significant impact of tau pathology on the dynamics of G4 DNA and on nuclear and nucleolar mechanobiology in neurons. These findings reveal new dimensions in the etiopathogenesis of tauopathies.

KEYWORDS

Alzheimer's disease, DNA, G quadruplex, nucleolus, nucleus, tau

This is an open access article under the terms of the [Creative Commons Attribution-NonCommercial-NoDerivs](https://creativecommons.org/licenses/by-nc-nd/4.0/) License, which permits use and distribution in any medium, provided the original work is properly cited, the use is non-commercial and no modifications or adaptations are made.

© 2024 The Authors. *Brain Pathology* published by John Wiley & Sons Ltd on behalf of International Society of Neuropathology.

1 | INTRODUCTION

The onset of tau protein aggregates in specific regions of the brain is a hallmark of tauopathies, the largest family of neurodegenerative diseases including Alzheimer's disease (AD). The progression of tau pathology in vulnerable neurons is associated with post-translational changes of tau monomers such as phosphorylation, and its progressive aggregation evolving to the formation of soluble tau oligomers, insoluble aggregates, paired helical filaments (PHF) and neurofibrillary tangles [1].

In vitro, the presence of nucleating agent is necessary to promote the polymerization of the intrinsically disordered tau monomers. In particular association with polyanions such as nucleic acids can promote the self-assembly of tau [2–4]. However, in vivo, involvement of nucleic acids in the tau aggregation process is still unclear. While the participation of RNA has been intensively studied [5–9], connections between DNA and the tau aggregation process has been only marginally investigated. Still, in AD hippocampi, DNA fragments have been recently identified in sarkosyl-insoluble aggregates including tau protein [10]. Interestingly DNA sequestered in the aggregates is significantly enriched in sequences predicted to form secondary guanine quadruplexes (G4) structures, questioning the involvement of G4-structured DNA (G4 DNA) in the pathology [10]. G4 are guanine-rich nucleic acid sequences which can fold and adopt various stable spatial conformations affecting DNA and RNA structuring and functions [11–13]. Notably, G4 play prevalent roles as regulators for gene expression and genomic stability [14–18]. In addition, G4 have been associated to protein folding and aggregation, and to neurodegenerative diseases including AD but their contribution in the progression of these pathologies is still largely underestimated [19–30].

In this study, we explored the impact of early and late stages of tau pathology on the distribution of G4 DNA in neurons from both transgenic mouse model of tau pathology THY-Tau22 (Tau22) [31] and human AD brains.

Our results reveal that early and late stages of tau pathology trigger strong disturbances in the dynamics of G4 DNA associated to multiple alterations in the morphology of the nuclear and nucleolar compartments, reflecting responses to stress likely to support neuronal survival.

2 | METHODS

2.1 | Animals

THY-Tau22 mouse (Tau22), and its nontransgenic littermates (WT) have been described in [31]. The Tau22 mouse was generated with a construct containing human tau46 mutated at G272V and P301S positions and

expressed under the control of Thy1.2 promoter. Tau pathology begins at 3 months of age in the subiculum and CA1 subfield, two brain regions affected early in human AD, spreading from there to the hippocampal dentate gyrus and cortex in older animals [32]. At 6 months of age, Tau22 mice start developing spatial memory impairment and anxiety [33]. All Tau22 mice used in the present study were heterozygous. Nontransgenic WT littermate mice were used as controls in all experiments. Both the THY-Tau22 and wild type littermate mice were generated from the same breeds. All mice were on C57Bl6/J background. Data from both males and females were analyzed as a single group. All animals were kept in standard animal cages (12 h/12 h light/dark cycle, at 22°C), with ad libitum access to food and water.

2.2 | Tissue collection

Adult human brain samples (C: $n = 5$; AD: $n = 5$) were obtained from the Lille Neurobank (Lille, France) (Table 1). Human brains from the Lille Neurobank were given to the French Research Ministry by the Lille University Hospital (CHRU-Lille) on August 14, 2008 under the reference DC-2000–642.

2.3 | Immunofluorescence (IF)

Murine sagittal or human coronal (5 μ M) brain slices were deparaffinized and unmasked using proteinase K at 20 μ g/mL in PBS 40 min at 37°C. After permeabilization for 10 min in PBS 0.2% Triton, slices were incubated with DNase-free RNase (50 μ g/mL in PBS, 90 min at 37°C) (Canvax EZ002). When specified, brains sections were incubated with DNase (Roche 10,104,159,001; 2 mg/mL in 10 mM Tris-HCl pH 7.5, 2.5 mM MgCl₂, 0.1 mM CaCl₂; 3 h at 37°C), or a mixture of RNase/DNase. The slices were submerged for 1 h in 1% goat serum (Vector Laboratories #S-1000) and the primary antibodies were incubated overnight at 4°C in the presence of PBS-0.2% Triton. Primary antibodies were revealed via secondary antibodies coupled to Alexa 488, 568 or 647 (Life Technologies) or anti human IgG (Fab specific) FITC conjugate (Sigma Aldrich F5512) for BG4. The sections were counterstained with 4',6-diamidino-2-phenylindole (DAPI) and mounted with fluorescence mounting medium (Agilent Dako S3023). The following antibodies were used: BG4 (anti-DNA/RNA G quadruplex; Absolute Antibody Ab00174-10.6), AT8 (PSer202/Thr205tau; ThermoFisher Scientific MN1020) (phospho-dependent antibody which is present from the early to late stages of tau pathology), TOC1 (anti-prefibrillar soluble tau oligomers; a generous gift from Dr. Nicholas Kanaan) [34], AT100 (recognizes tau phosphorylated at epitope Ser212/Thr214, and aggregated in sarkosyl-insoluble PHF; ThermoFisher Scientific MN1060) [35], nucleolin

TABLE 1 Braak scores, region, age, gender, and post mortem interval of the brains.

	Braak score	Tissue	Age	Sex	PMI (hours)
C#1	I	Frontal cortex	69	M	21
C#2	0	Frontal cortex	74	M	48
C#3	I	Frontal cortex	90	F	16
C#4	0	Frontal cortex	62	M	60
C#5	0	Frontal cortex	64	F	30
AD#1	VI	Frontal cortex	76	F	22
AD#2	VI	Frontal cortex	67	M	36
AD#3	VI	Temporal cortex	73	F	5.5
AD#4	VI	Occipital cortex	86	F	8
AD#5	VI	Temporal cortex	61	M	23

Note: Anonymized data.

Abbreviation: PMI, postmortem interval.

(ThermoFisher Scientific A300-711-A), 8-OHdG (8-oxo-G)(anti-8-hydroxy-2'-deoxyguanosine and 8-hydroxyguanosine; ThermoFisher Scientific BS-1278R). DAPI were used as a chromatin counterstain. Nuclear (based on DAPI) and nucleolar (based on nucleolin detection) labeling of cells were quantified using the FIDJI macro application of ImageJ (confocal microscopy platform, PBSL, UAR2014/US41, Lille). Quantification corresponds to the z stack of serial confocal sections covering the entire thickness of the brain section. The quantification shows the mean of nuclear fluorescence values per individual. Fluorescence from human brain sections (C $n = 5$; AD $n = 5$) and mouse brain sections (Tau22 $n = 26$, WT $n = 13$; KOTau $n = 14$, WT $n = 16$) was acquired using an LSM 710 and an LSM 980 confocal laser-scanning microscopes (Carl Zeiss). The confocal microscope was equipped with a 488-nm Argon laser, 561-nm diode-pumped solid-state laser, and a 405-nm ultraviolet laser. The images were acquired using ZEN software (Carl Zeiss). The images were acquired using a 20 \times /0,8 and an oil 63 \times /1,4 Plan-APOCHROMAT objective. All recordings were performed using the appropriate sampling frequency (16 bits, optimal sampling, and a line average of 4). 3D reconstruction was performed using Bitplane Imaris software (Oxford Instruments). To achieve optimal z-sampling, acquisitions were carried out using Z-steps of 0.2 μ m. Imaris 3D surfaces is use to precisely visualize and measure shapes of various objects and identify highlight the marked surfaces in the images.

2.4 | Statistics for IF analysis

The Shapiro–Wilk test of normality (GraphPad Prism 7) was used to test if the data were normally distributed. Two-tailed, unpaired Student's *t*-test (parametric) or Mann Whitney U test (nonparametric) (GraphPad Prism 7) were used for statistical analysis of IF and statistical

analysis of the nuclear and nucleolar area. Each biological replicate corresponds to one mouse brain. The number of biological replicates is indicated in the legends. The experimenters were not blinded. Data are presented as mean \pm SEM, * $p < 0.05$; ** $p < 0.01$; *** $p < 0.001$; **** $p < 0.0001$.

3 | RESULTS

3.1 | G4 DNA colocalizes with nucleoli and heterochromatin in CA1 neurons from wild type mice

We first analyzed by IF the presence of G4 DNA structures in hippocampal CA1 neurons in sagittal sections from 6-months-old (6 m) WT control mice using the BG4 antibody [36, 37]. As the BG4 antibody recognizes G4 sequences both in DNA and RNA, brain sections were pre-incubated with DNase-free RNase (RNase) prior to BG4, to specifically investigate the presence of G4 DNA in neurons (Figures 1A,B and S1A). BG4 labeling appeared as an heterogeneous distribution restricted to nuclei. BG4 IF was mostly detected as dense circular foci, coinciding with a dark hole in the DAPI staining and near DAPI spots reminiscent of perinucleolar heterochromatin, suggesting that it corresponds to a nucleolar location (Figure 1A, closed arrowhead; Figures 1B and S1A). To verify this hypothesis, double labeling using the BG4 antibody and antibody directed against the nucleolar protein nucleolin was performed (Figure 1C). The clear codistribution of BG4 and nucleolin labelings showed that G4 DNA sequences are highly present in neuronal nucleoli in hippocampal neurons (Figure 1C,D). In addition, BG4 IF was present on but mainly with a patchy distribution around DAPI spots, which correspond to highly packed heterochromatin foci (Figure 1A, empty arrowhead; Figures 1B and S1A). Thus, it indicates that G4 DNA sequences are enriched at the periphery of

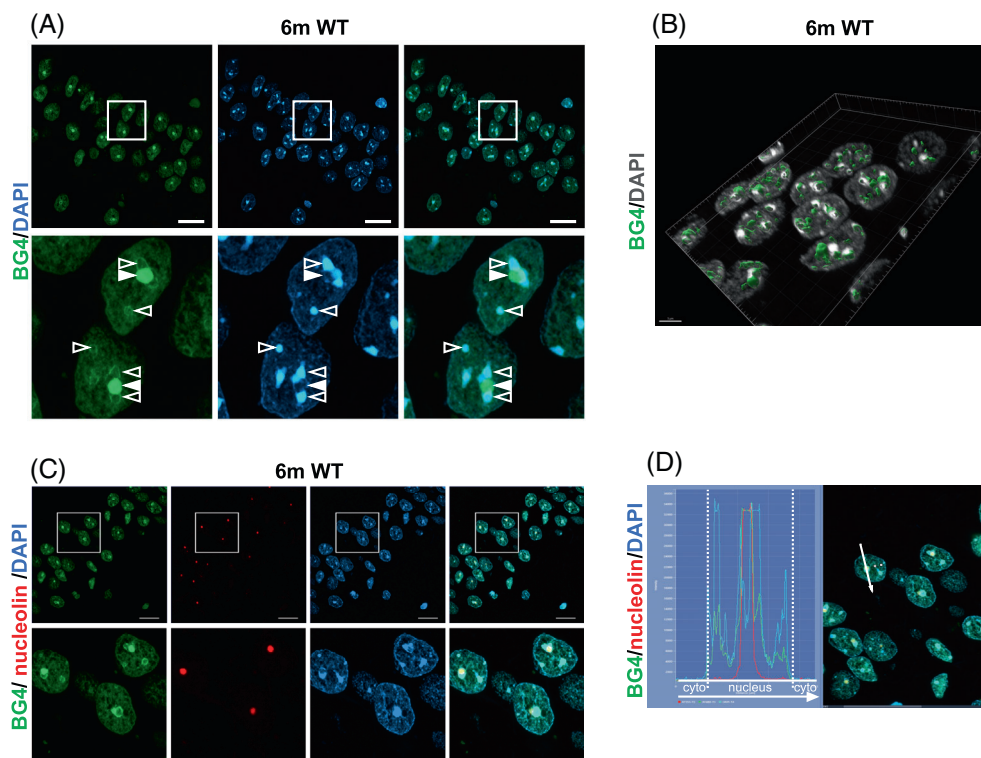


FIGURE 1 G4 DNA structures are concentrated within the nucleoli and around heterochromatin foci in neuronal nuclei. (A) Representative images of sagittal sections from 6 m WT mice ($n = 5$). The sections were labeled with the BG4 antibody. IF signals were analyzed by confocal laser-scanning microscopy (z projection). Nuclei were detected with DAPI staining. The scale bars represent 20 μm . Closed arrowheads show dense BG4 positive spots near heterochromatin foci. Empty arrowheads show BG4 labeling around heterochromatin foci. (B) 3D images reconstruction of sagittal sections from 6 m WT mice ($n = 5$). IF signals were analyzed by confocal laser-scanning microscopy. Nuclei were detected with DAPI staining (gray). The sections were labeled with the BG4 antibody (green). Imaris 3D Surface module were used to indicate heterogeneous distribution of BG4 labeling in nuclei. The scale bar represents 5 μm . (C) Representative images of sagittal sections from 6 m WT mice ($n = 5$). The sections were labeled with the BG4 and nucleolin antibodies. IF signals were analyzed by confocal laser-scanning microscopy (z projection). Nuclei were detected with DAPI staining. The scale bars represent 20 μm . (D) Right panel: The indicated white arrow is drawn across nucleus and nucleolus in a confocal section of CA1 neurons from 6 m WT mice. Left panel: Quantification of the fluorescence signals for BG4, nucleolin and DAPI along the indicated arrow scan. The cell cytoplasm (cyto) and nucleus are delimited by dashed lines.

heterochromatin structures. A lattice distribution was also observed throughout the nucleus partly codistributed with DAPI signal (Figures 1A,B and S1A).

Most of the BG4 signal was abolished by pretreatment with DNase indicating that nuclear G4 are mainly secondary DNA structures in hippocampal neurons (Figure S1B). Concomitant RNase and DNase pretreatments prevented BG4 labeling confirming the specificity of BG4 for nucleic acid structures (Figure S1B).

In the rest of the study, brain sections were systematically preincubated with RNase prior to incubation with BG4, to visualize G4 DNA specifically.

3.2 | Early stages of tau pathology trigger aberrant cytoplasmic accumulation of G4 DNA in a subpopulation of CA1 neurons from 6-months-old Tau22 mice

We first investigated the impact of early stages of tau pathology on neuronal G4 DNA distribution in the transgenic mouse model THY-Tau22 (Tau22) at the

onset of cognitive deficits [33]. G4 DNA location was analyzed in hippocampal CA1 neurons from 6 m Tau22 transgenic and WT littermate mice, using the BG4 antibody without (Figure 2A,B) or with nucleolin antibody (Figure S2A). The majority of CA1 neurons from 6 m Tau22 mice, exhibited only nuclear localization of BG4 labeling (cyto BG4⁻ neurons), with preponderance at the nucleolus as for WT neurons (Figures 2A and S2A). Surprisingly, BG4 labeling was also detected in the cytoplasm of a subpopulation of neurons (cyto BG4⁺ neurons) (Figures 2A,B and S2A, arrowheads). Noteworthy, a redistribution of the nuclear BG4 labeling is clearly visible in some of the cyto BG4⁺ neurons (Figure 2A, zoom; 2B). Nucleolar BG4 and nucleolin labelings even disappeared in some of the cyto BG4⁺ neurons (Figure S2A, empty arrowheads).

DAPI fluorescence was detected in the cytoplasm of cyto BG4⁺ neurons (Figure 2C) showing the existence of DNA in the cytoplasm. The overexposure of the DAPI fluorescent signal clearly revealed a cytoplasmic staining specifically codistributed with BG4 labeling (Figure 2D).

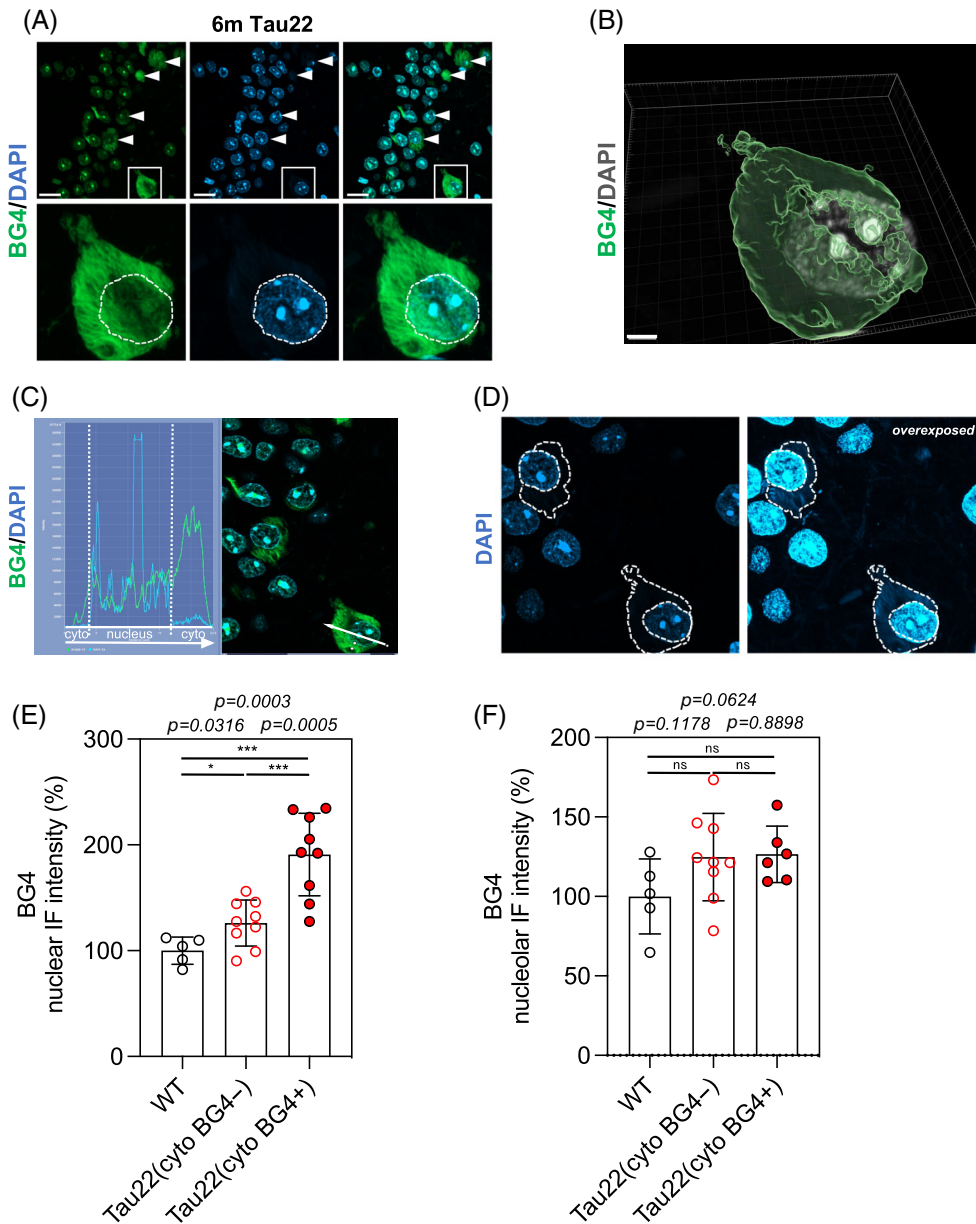


FIGURE 2 G4 DNA redistribution and morphological changes in a subpopulation of neurons in 6 m Tau22 mouse brains. (A) Representative images of sagittal sections from 6 m WT and Tau22 mice (WT: $n = 5$; Tau22: $n = 9$). The sections were labeled with the BG4 antibody. IF signals were analyzed by confocal laser-scanning microscopy (z projection). Nuclei were detected with DAPI staining. The scale bars represent 20 μm. Arrowheads and frames show neurons with cytoplasmic G4 DNA accumulation. Dashed lines delimitate the nucleus. (B) 3D images reconstruction of sagittal sections from 6 m Tau22 mice ($n = 9$). IF signals were analyzed by confocal laser-scanning microscopy. Nuclei were detected with DAPI staining (gray). The sections were labeled with the BG4 antibody (green). Imaris 3D Surface module were used to indicate heterogeneous distribution of BG4 labeling in neuron. The scale bar represents 3 μm. (C) Right panel: the indicated arrow is drawn across neuron in a confocal section of CA1 from 6 m Tau22 mice. Left panel: quantification of the fluorescence signals for BG4 and DAPI along the indicated arrow scan. The cell cytoplasm (cyto) and nucleus are delimited by dashed lines. (D) Left panel: DAPI staining in a confocal section of neurons from 6 m Tau22 mice. Dashed lines delimitate the cytoplasm and nucleus. Right panel: DAPI fluorescence signal has been overexposed to reveal cytoplasmic DAPI staining in a subpopulation of neurons. (E) The intensity of the nuclear BG4 IF signal was separately quantified within neurons ($n = 124$) from WT mice ($n = 5$) and within cyto BG4- ($n = 144$) and cyto BG4+ ($n = 46$) neurons from the same Tau22 mice ($n = 9$). Graph shows the mean of nuclear BG4 fluorescence per category. Each biological replicate corresponds to one mouse. Data are presented as mean \pm SEM (* $p < 0.05$; *** $p < 0.001$; Two-tailed, unpaired Student's t -test). (F) The intensity of the nucleolar BG4 IF signal was separately quantified within neurons ($n = 167$) from WT mice ($n = 5$) and within cyto BG4- ($n = 199$) and cyto BG4+ ($n = 18$) neurons from the same Tau22 mice ($n = 9$). Note that nucleoli were not detected in cyto BG4+ neurons in three of the nine mice. Graph shows the mean of nucleolar BG4 fluorescence per category. Each biological replicate corresponds to one mouse. Data are presented as mean \pm SEM (ns = nonsignificant; Two-tailed, unpaired Student's t -test).

Supplementary pretreatment of the brain sections with DNase fully prevented the cytoplasmic BG4 labeling, demonstrating the absence of nonspecific BG4 binding into the cytoplasm (Figure S2B).

Taken together, these data reveal the presence of G4 DNA in the cytoplasm of a subpopulation of CA1 neurons from 6 m Tau22 mice.

Quantification showed an increase in the mean G4 DNA level into the nuclei of 6 m Tau22 compared with WT neurons, with a stronger effect observed in cyto BG4+ compared with cyto BG4- neurons (Figure 2E), in contrast, there was no statistically different nucleolar G4 DNA contents in cyto BG4- and cyto BG4+ neurons from 6 m Tau22 compared with WT littermate neurons (Figure 2F).

Altogether these results show that the nuclear level of G4 DNA starts to increase in the nucleus before G4 DNA appears in the cytoplasm of cyto BG4+ CA1 neurons. This suggests that cyto BG4- neurons reflect an earlier phase of the disease than cyto BG4+ neurons, corresponding to a precocious stage of tau pathology.

3.3 | Tau hyperphosphorylation, tau oligomerization, and oxidative DNA damage precede cytoplasmic G4 DNA accrual in CA1 neurons

In 6 m Tau22 mice the onset of cognitive deficits coincides with increased tau phosphorylation and an enrichment with soluble oligomeric forms of tau in hippocampal CA1 neurons [33,38,39]. We next analyzed the relationship between the presence of phosphorylated forms of tau (P-tau) or tau oligomers and the distribution of G4 DNA. We performed double labeling using AT8 or TOC1 antibodies which recognize phosphorylated Ser202/Thr205 tau and soluble tau oligomers, respectively [40], and the BG4 antibody (Figure 3A,D). Strikingly, the accumulation of P-tau or tau oligomers was detected in all cyto BG4+ neurons (Figure 3A,D, closed arrowheads; Figure 3B,E). In contrast, only part of neurons positive for P-tau or tau oligomers showed cytoplasmic BG4 labeling (Figure 3A,D, empty arrowheads; Figure 3C,F). Thus, accumulation of G4 DNA in the cytoplasm is not mandatory to tau hyperphosphorylation and oligomerization.

Altogether these results suggest that the abnormal presence of G4 DNA in the cytoplasm of neurons is a downstream event of early tau hyperphosphorylation and oligomerization.

We previously described that CA1 neurons from 6 m Tau22 mice undergo a transient increase in oxidative stress [39]. Because of the lower redox potential of guanine, G4 are highly susceptible to oxidative damage

[41, 42]. We therefore investigated the interplay between guanine oxidation and G4 DNA in CA1 neurons from Tau22 and WT littermate mice by IF using an antibody against 8-hydroxy-2'-deoxyguanosine (8-oxo-G), an oxidized form of guanosine and typical marker of oxidative DNA damage, and the BG4 antibody. Oxidative DNA damage was closely associated to the presence of G4 DNA in the cytoplasm of cyto BG4+ neurons in 6 m Tau22 mice (Figure 4A, closed arrowheads; Figure 4B). However, oxidative DNA damage was also present in the cytoplasm of some cyto BG4- neurons (Figure 4A, empty arrowheads; Figure 4C).

Thus, it suggests that cytoplasmic G4 DNA accumulation in neurons is a downstream event of guanine oxidation and consequently of oxidative stress.

3.4 | G4 DNA redistribution coincides with morphological alterations of the nuclear and nucleolar compartments

As various cellular stresses including oxidative stress can alter the nuclear and nucleolar morphology, we analyzed the size of nuclei and nucleoli in CA1 neurons from 6 m Tau22 and WT littermate mice.

Based on the area of the DAPI staining, we observed a statistically significant reduction in the mean nuclear size specifically in cyto BG4+ neurons from 6 m Tau22 compared with cyto BG4- and WT littermate neurons (Figure 4D). The shrinkage of the nuclei is therefore associated with the presence of G4 DNA in the cytoplasm.

In addition, as our previous results showed that oxidative stress is an upstream event in the cytoplasmic localization of G4 DNA, we separately analyzed nuclear size in neurons without and with oxidative DNA damage prior to the appearance of G4 DNA in the cytoplasm (cyto 8oxoG- BG4- and cyto 8oxoG+ BG4- neurons respectively) (Figure 4E). The presence of oxidized DNA in the cytoplasm in the absence of G4 DNA (cyto 8oxoG+ BG4- neurons), is not associated with a reduction in the nuclear size showing that oxidative DNA damage alone does not cause nuclear shrinkage.

Surprisingly, based on the area of the nucleolin labeling [43], we observed a statistically significant increase in the mean nucleolus size in cyto BG4- neurons from 6 m Tau22 compared with WT littermate neurons (Figure 4F). The mean nucleolus size in cyto BG4+ neurons was no longer different from that in WTs, although there was considerable variability between mice (Figure 4F).

These data suggest that, in CA1 neurons from 6 m Tau22 mice, nucleolar hypertrophy occurs transiently, prior to cytoplasmic G4 DNA accumulation associated to nuclear shrinkage. Altogether, it shows that the nuclear and nucleolar morphology is impaired in a non-synchronous way at early stages of tau pathology.

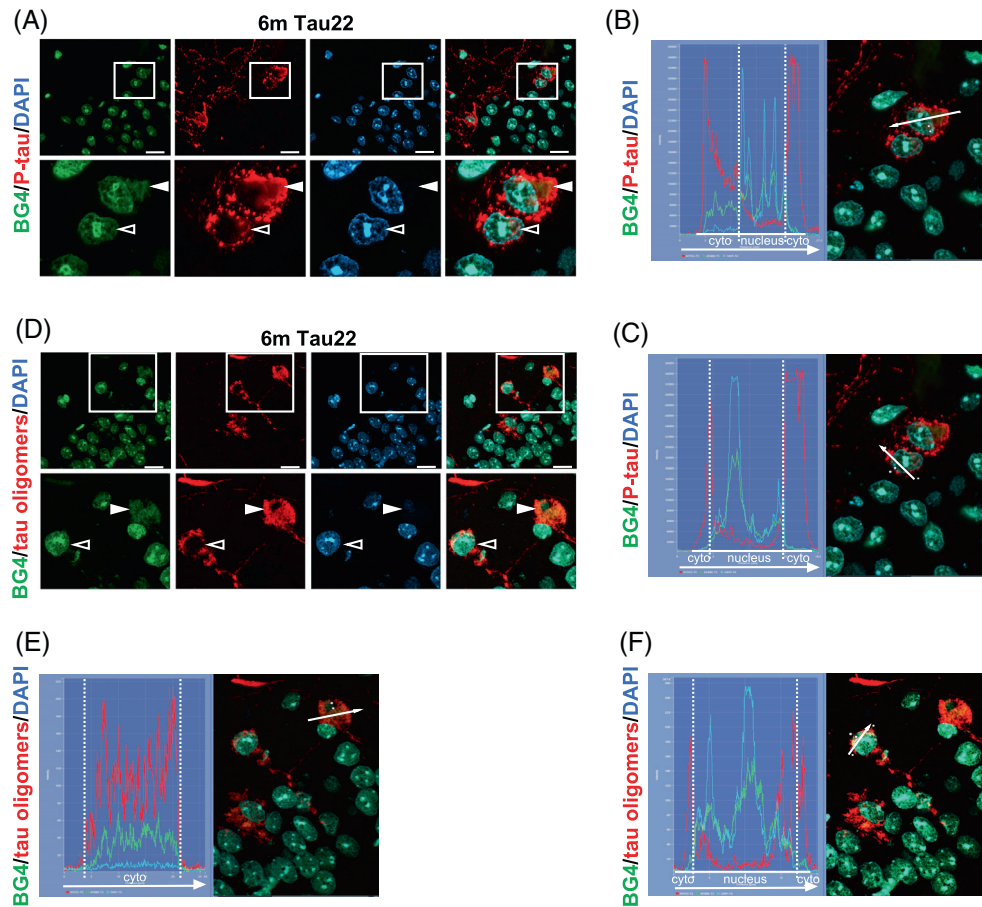


FIGURE 3 Cytoplasmic G4 DNA is associated with phosphorylated and oligomerized tau in a subpopulation of neurons from 6 m Tau22 mouse brains. (A) Representative images of sagittal sections from 6 m Tau22 mice (WT: $n = 5$; Tau22: $n = 9$). The sections were labeled with the BG4 and anti-P-tau (AT8) antibodies. IF signals were analyzed by confocal laser-scanning microscopy (z projection). Nuclei were detected with DAPI staining. The scale bars represent 20 μm . Closed arrowheads show cyto BG4+ neuron. Empty arrowheads show cyto BG4- neuron. (B) Right panel: The indicated arrow is drawn across cyto BG4+ neuron in a confocal section of CA1 from 6 m Tau22 mice. Left panel: Quantification of the fluorescence signals for BG4, P-tau, and DAPI along the indicated arrow scan. The cell cytoplasm (cyto) and nucleus are delimited by dashed lines. Graph shows the colocalization of G4 DNA with P-tau into the cytoplasm. (C) Right panel: The indicated arrow is drawn across cyto BG4- neuron in a confocal section of CA1 from 6 m Tau22 mice. Left panel: Quantification of the fluorescence signals for BG4, P-tau, and DAPI along the indicated arrow scan. The cell cytoplasm (cyto) and nucleus are delimited by dashed lines. Graph shows the absence of G4 DNA in the cytoplasm of neuron with P-tau. (D) Representative images of sagittal sections from 6 m Tau22 mice (WT: $n = 5$; Tau22: $n = 9$). The sections were labeled with the BG4 and anti-tau oligomers (TOC1) antibodies. IF signals were analyzed by confocal laser-scanning microscopy (z projection). Nuclei were detected with DAPI staining. The scale bars represent 20 μm . Closed arrowheads show cyto BG4+ neuron. Empty arrowheads show cyto BG4- neuron. (E) Right panel: The indicated arrow is drawn across cyto BG4+ neuron in a confocal section of CA1 from 6 m Tau22 mice. Left panel: Quantification of the fluorescence signals for BG4, tau oligomers and DAPI along the indicated arrow scan. The cell cytoplasm (cyto) is delimited by dashed lines. Graph shows the colocalization of G4 DNA with tau oligomers into the cytoplasm. (F) Right panel: The indicated arrow is drawn across cyto BG4- neuron in a confocal section of CA1 from 6 m Tau22 mice. Left panel: Quantification of the fluorescence signals for BG4, tau oligomers and DAPI along the indicated arrow scan. The cell cytoplasm (cyto) and nucleus are delimited by dashed lines. Graph shows the absence of G4 DNA in the cytoplasm of neuron with tau oligomers.

3.5 | Late tau pathology is associated with persistence of cytoplasmic G4 DNA deposition, reduction of nuclear and nucleolar G4 DNA load, and nucleolar compaction in CA1 neurons from 12-months-old Tau22 mice

Tau pathology peaks when Tau22 mice are 12-months old (12 m). We next investigated by IF the impact of late tau pathology on the distribution of G4 DNA and on the nuclear and nucleolar morphology in CA1 neurons from 12 m Tau22 transgenic mice and WT littermates,

using the BG4 antibody without or with nucleolin antibody.

The distribution of G4 DNA in neurons from 12 m WT mice was similar to that in neurons from 6 m mice (Figures 5A and S3A). This indicates that the cytoplasmic localization previously observed in neurons from 6 m Tau22 mice does not reflect accelerated aging. Cytoplasmic accumulation of G4 DNA persisted in neurons of 12 m Tau22 mice as tau pathology worsens (Figure 5A, arrowheads; Figure S3A). In addition the number of neurons with cytoplasmic G4 DNA doubled in 12 m mice

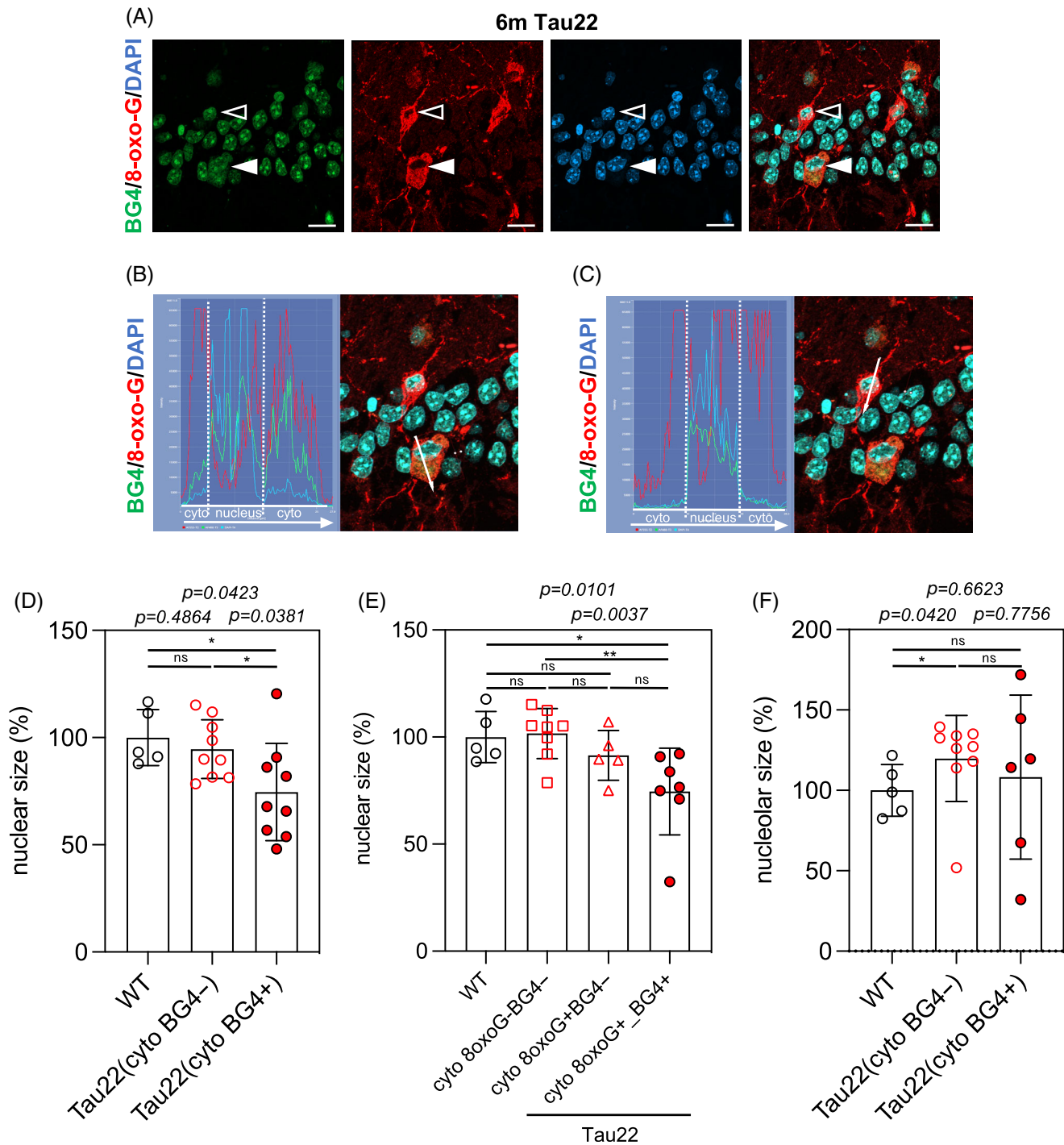


FIGURE 4 Legend on next page.

compared with 6 m mice (cyto BG4+/total neurons: 6 m = 7.93%; 12 m = 16.74%) (Figure 5B).

Late tau pathology had no effect on the nuclear G4 DNA level (Figure S3B) despite a reduction in the nuclear size in cyto BG4+ neurons compared with cyto BG4- and WT neurons (Figure S3C). In contrast, quantification revealed a strong decrease of the nucleolar G4 DNA load (Figure 5C) associated to a reduction in the

nucleolar size (Figure 5D) in cyto BG4+ neurons from 12 m Tau22 compared with cyto BG4- and WT neurons.

Altogether our results highlight reduction of the nucleolar G4 DNA load associated with nuclear and nucleolar shrinkage, selectively in neurons containing cytoplasmic G4 DNA deposition at late stage of tau pathology.

Late tau pathology is characterized by the predominance of hyperphosphorylated and aggregated forms of tau in CA1 neurons of Tau22 mice [39]. We next analyzed by IF the connection between the presence of phosphorylated and aggregated forms of tau and the G4 DNA distribution using the AT100 antibody, which recognizes tau phosphorylated at epitope Ser212/Thr214 and aggregated in sarkosyl-insoluble PHF [35], and the BG4 antibody respectively. The accumulation of phosphorylated tau aggregates was detected in all the cyto BG4+ neurons (Figure 5E, closed arrowheads; Figure 5F(a)) showing the persistent association between cytoplasmic G4 DNA and pathogenic forms of tau at late stage of tau pathology. Phosphorylated tau aggregates was also present in the cytoplasm of some of the cyto BG4- neurons (Figure 5E, open arrowheads; Figure 5F(b)) confirming that the presence of G4 DNA in the cytoplasm is not critical to the tau aggregation process.

As we previously described [39], oxidative DNA damage was no more increased in CA1 neurons from 12 m Tau22 compared with WT littermate mice (data not shown).

3.6 | Tau deletion has no effect on G4 DNA distribution in CA1 neurons

In addition, we tested the effect of the absence of tau on the distribution of G4 DNA in CA1 neurons from tau deficient (KOTau) and WT littermate mice. Tau deletion induced neither cytoplasmic location of G4 DNA nor change of nuclear G4 DNA level in 12 m CA1 KOTau compared with WT neurons (Figure S4A,B). These data suggest that alterations in the distribution of G4 DNA observed in Tau22 neurons are not the result of a loss of tau function but are rather linked to a gain in toxic function induced by tau pathology, although we cannot rule

out the possibility of compensatory mechanisms being set up in KOTau neurons.

3.7 | Impaired G4 DNA dynamics is associated to pathogenic forms of tau and oxidative DNA damage in neurons from AD brains

We next investigated the relevance of the association between pathogenic forms of tau, oxidative DNA damage and alteration of the G4 DNA distribution in postmortem AD (Braak 6) compared with aged-matched nondemented (control) cerebral cortex. Coronal sections of cortex were labeled with AT8 (P-tau), TOC1 (tau oligomers), AT100 (aggregated P-tau), or anti-8-oxo-G (oxidative DNA damage) antibodies, and with the BG4 antibody. In control brains, G4 DNA was distributed on and around DAPI foci corresponding to heterochromatin, and in non-DAPI-labeled cavities indicating nucleoli (Figure S5), similarly to what we observed in murine neurons. It is worth noting that cytoplasmic presence of G4 DNA was weakly detected in some cortical cells from certain control brains (Figure S5, stars) possibly reflecting an effect of aging.

Cytoplasmic accumulation of G4 DNA was found in subpopulations of neurons containing hyperphosphorylated, oligomerized and/or aggregated forms of tau in cortex from human AD brains (Figure 6A–C). Similarly, G4 DNA was associated to oxidative DNA damage in the cytoplasm of AD cortical neurons (Figure 6D). Phosphorylated, oligomerized or aggregated forms of tau, and oxidized DNA were not detected in the cytoplasm of control brains (data not shown) as previously described [39, 44].

Thus, these results demonstrate the connection between pathogenic forms of tau and oxidative DNA damage, and a severe redistribution of G4 DNA in cortical neurons from AD brains.

FIGURE 4 Cytoplasmic G4 DNA and oxidative DNA damage are present in a subpopulation of neurons from 6 m Tau22 mouse brains. (A) Representative images of sagittal sections from 6 m Tau22 mice (WT: $n = 5$; Tau22: $n = 9$). The sections were labeled with the BG4 and anti-8-oxo-G antibodies. IF signals were analyzed by confocal laser-scanning microscopy (z projection). Nuclei were detected with DAPI staining. The scale bars represent 20 μm . Closed arrowheads show cyto BG4+ neuron. Empty arrowheads show cyto BG4- neuron. (B) Right panel: the indicated arrow is drawn across cyto BG4+ neuron in a confocal section of CA1 from 6 m Tau22 mice. Left panel: quantification of the fluorescence signals for BG4, 8-oxo-G, and DAPI along the indicated arrow scan. The cell cytoplasm (cyto) and nucleus are delimited by dashed lines. Graph shows the colocalization of G4 DNA with P-tau into the cytoplasm. (C) Right panel: the indicated arrow is drawn across cyto BG4- neuron in a confocal section of CA1 from 6 m Tau22 mice. Left panel: Quantification of the fluorescence signals for BG4, 8-oxo-G, and DAPI along the indicated arrow scan. The cell cytoplasm (cyto) and nucleus are delimited by dashed lines. Graph shows the absence of cytoplasmic G4 DNA in neuron with P-tau. (D) The nuclear area was separately quantified within neurons ($n = 124$) from WT mice ($n = 5$) and within cyto BG4- ($n = 144$) and cyto BG4+ ($n = 46$) neurons from the same Tau22 mice ($n = 9$). Graph shows the mean of nuclear area per category. Each biological replicate corresponds to one mouse. Data are presented as mean \pm SEM (ns = nonsignificant; * $p < 0.05$; Two-tailed, unpaired Student's t -test). (E) The nuclear area was separately quantified within neurons ($n = 91$) from WT mice ($n = 5$) and within cyto 8oxoG- BG4- ($n = 139$), cyto 8oxoG+ BG4- ($n = 19$), and cyto 8oxoG+ BG4+ ($n = 25$) neurons from the same Tau22 mice ($n = 5$ –8). Graph shows the mean of nuclear area per category. Each biological replicate corresponds to one mouse. Data are presented as mean \pm SEM (ns = nonsignificant; * $p < 0.05$, ** $p < 0.01$, Mann-Whitney test). (F) The nucleolar area was separately quantified within neurons ($n = 167$) from WT mice ($n = 5$) and within cyto BG4- ($n = 199$) and cyto BG4+ ($n = 18$) neurons from the same Tau22 mice ($n = 9$). Note that nucleoli were not detected in cyto BG4+ neurons in three of the nine mice. Graph shows the mean of nucleolar area per category. Each biological replicate corresponds to one mouse. Data are presented as mean \pm SEM (* $p < 0.05$, Mann-Whitney test; ns = nonsignificant, Two-tailed, unpaired Student's t -test).

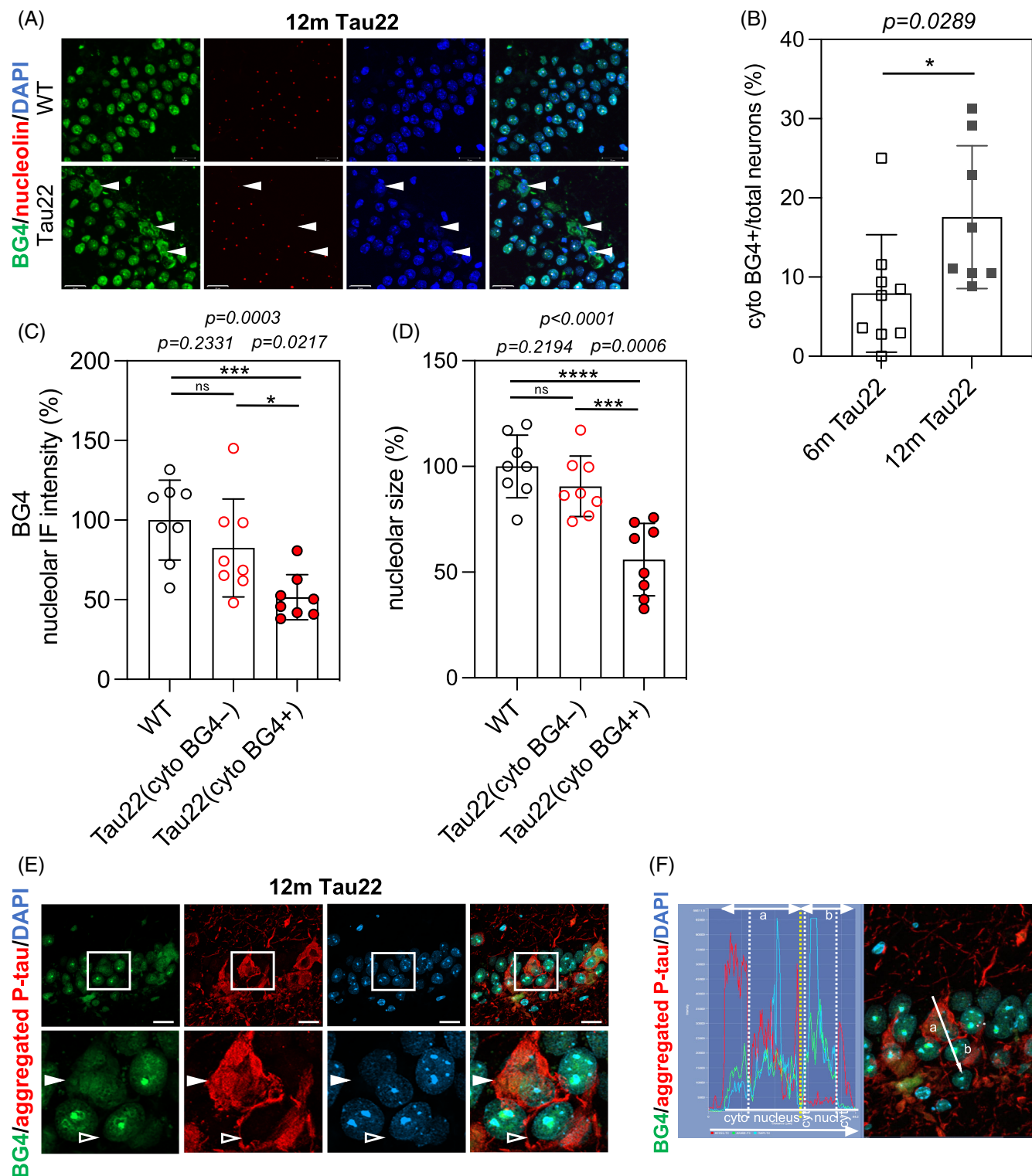


FIGURE 5 Legend on next page.

4 | CONCLUSIONS

These results link early and late stages of tau pathology to major changes in the cellular distribution of G4 DNA associated to various morphological alterations of nuclei and nucleoli in neurons (Figure 7A).

4.1 | G4 DNA distribution in healthy neurons

Although highly studied in cellular models, G4 (DNA and RNA) had only recently been visualized in vivo in hippocampal neurons from mouse brains [45]. Here, we report a nuclear distribution of G4 DNA in healthy

neurons, with a high density in nucleoli likely reflecting an enrichment of G4 structures in ribosomal DNA (rDNA), although nonribosomal DNA is also present [46]. This is in agreement with the abundance of rDNA sequences prone to form G4 into nucleoli that has been predicted by whole genome analysis [47–49].

In addition, we describe patchy enrichment of G4 DNA around heterochromatin foci. The presence of G4 structures at the heterochromatin level was previously documented in murine hippocampal neurons [45] and more generally in several somatic cell types [50, 51]. Here, the specific enrichment of G4 DNA at the periphery of heterochromatin foci questions its role. In particular, it would be interesting to investigate if this special location, reminiscent of a wire mesh, reflects a role in chromatin compaction.

Nevertheless, as our study is based on the use of the BG4 antibody it should be stressed that, despite being the reference antibody for G4 detection, controversy about its specificity has recently been reported. Ray et al. [52] have shown that BG4 can also recognize non-G4 motifs including cytosine-rich sequences. We cannot therefore rule out the possibility that part of the BG4 signal detected in our study corresponds to DNA structures other than G4. Nevertheless, the use of a fluorescence probe that specifically recognizes G4 DNA structures in fixed tissue would be beneficial as an additional method of detection [53].

4.2 | Impaired G4 DNA dynamics in neurons: Potential causes and consequences

In AD brains, Shmookler Reis et al. described the presence of predicted G4-forming DNA sequences, mainly of nuclear origin, in sarkosyl-insoluble extracts containing tau aggregates [10]. Here, our results provide the first visualization of G4 DNA codistributed with soluble

oligomers and larger aggregated forms of tau in the cytoplasm of murine and human AD neurons. But the origin of DNA structured in G4 present in the cytoplasm of neurons from Tau22 mice and AD brains remains to be identified.

A key future challenge will be to elucidate molecular mechanisms underlying the dysregulation of G4 DNA dynamics in neurons and to highlight its impact for neuronal homeostasis. Numerous mechanisms can lead to the presence of DNA into the cytoplasm of cells [54]. Our results suggest that the cytoplasmic location of G4 DNA is secondary to the presence of oligomers or larger aggregated forms of tau. This implies that the abnormal presence of G4 DNA in the cytoplasm does not have a causal role in driving the aggregation process but is rather a downstream event. Tau protein can undergo liquid–liquid phase separation (LLPS) to form tau droplets promoting tau aggregation [4,55–59]. Recently, Gao et al. showed that LLPS can modulate G4 DNA formation and stability [60]. Therefore it is plausible that LLPS process linked to tau aggregation may favor G4 structuring of guanine-rich DNA sequences. Conversely, as G4 structuring can possibly accelerate protein folding, notably promoting LLPS [25,26], it cannot be ruled out that once present in the cytoplasm, G4 DNA may exacerbate the tau aggregation process. The relationship between tau aggregation, LLPS and G4 DNA in neurons warrants further investigation.

In this and previous studies we report that in 6 m Tau22 mice, when tau oligomers are predominant, CA1 neurons are facing stress including oxidative stress [39]. Here, our results suggest that the prevalence of cytoplasmic G4 DNA is a downstream event of oxidative stress in neurons. Interestingly, Byrd et al. reported that oxidative stress can promote G4 DNA location in the cytoplasm of cell lines [61]. Thus, oxidative stress could participate in cytoplasmic location of G4 DNA in neurons. Oxidative DNA damage can lead to DNA breaks and the

FIGURE 5 Altered distribution of G4 DNA persists in CA1 neurons from 12 m Tau22 mice. (A) Representative images of sagittal sections from 12 m WT ($n = 8$) and Tau22 ($n = 17$) mice. The sections were labeled with the BG4 and nucleolin antibodies. IF signals were analyzed by confocal laser-scanning microscopy (z projection). Nuclei were detected with DAPI staining. The scale bars represent 20 μm . Closed arrowheads show cyto BG4+ neurons. (B) The percentage of cyto BG4+ neurons was separately quantified within neurons ($n = 388$) from 6 m Tau22 mice ($n = 9$) and within neurons ($n = 403$) from 12 m Tau22 mice ($n = 8$). Graph shows the mean percentage of cyto BG4+ neurons among the total number of neurons per category. Each biological replicate corresponds to one mouse. Data are presented as mean \pm SEM (* $p < 0.05$; Two-tailed, unpaired Student's *t*-test). (C) The intensity of the nucleolar BG4 IF signal was separately quantified within neurons ($n = 105$) from WT mice ($n = 8$) and within cyto BG4– ($n = 166$) and cyto BG4+ ($n = 46$) neurons from the same 12 m Tau22 mice ($n = 8$). Graph shows the mean of nuclear BG4 fluorescence per category. Each biological replicate corresponds to one mouse. Data are presented as mean \pm SEM (ns = nonsignificant; * $p < 0.05$; *** $p < 0.001$; Two-tailed, unpaired Student's *t*-test). (D) The nucleolar area was separately quantified within neurons ($n = 105$) from WT mice ($n = 8$) and within cyto BG4– ($n = 166$) and cyto BG4+ ($n = 46$) neurons from the same 12 m Tau22 mice ($n = 8$). Graph shows the mean of nucleolar area per category. Each biological replicate corresponds to one mouse. Data are presented as mean \pm SEM (ns = nonsignificant; *** $p < 0.001$; **** $p < 0.0001$; Two-tailed, unpaired Student's *t*-test). (E) Representative images of sagittal sections from 12 m Tau22 mice (WT: $n = 8$; Tau22: $n = 8$). The sections were labeled with the BG4 and anti-aggregated P-tau (AT100) antibodies. IF signals were analyzed by confocal laser-scanning microscopy (z projection). Nuclei were detected with DAPI staining. The scale bars represent 20 μm . Closed arrowheads show cyto BG4+ neuron. Empty arrowheads show cyto BG4– neuron. (F) Right panel: The indicated arrow is drawn across cyto BG4+ (a) and cyto BG4– (b) neurons in a confocal section of CA1 from 12 m Tau22 mice. Left panel: Quantification of the fluorescence signals for BG4, aggregated P-tau and DAPI along the indicated arrow scan. The cell cytoplasm (cyto) and nucleus are delimited by dashed lines. Graph shows the codistribution of G4 DNA with aggregated P-tau into the cytoplasm of a cyto BG4+ neuron (a) and the absence of G4 DNA in the cytoplasm of a cyto BG4– neuron with aggregated P-tau (b).

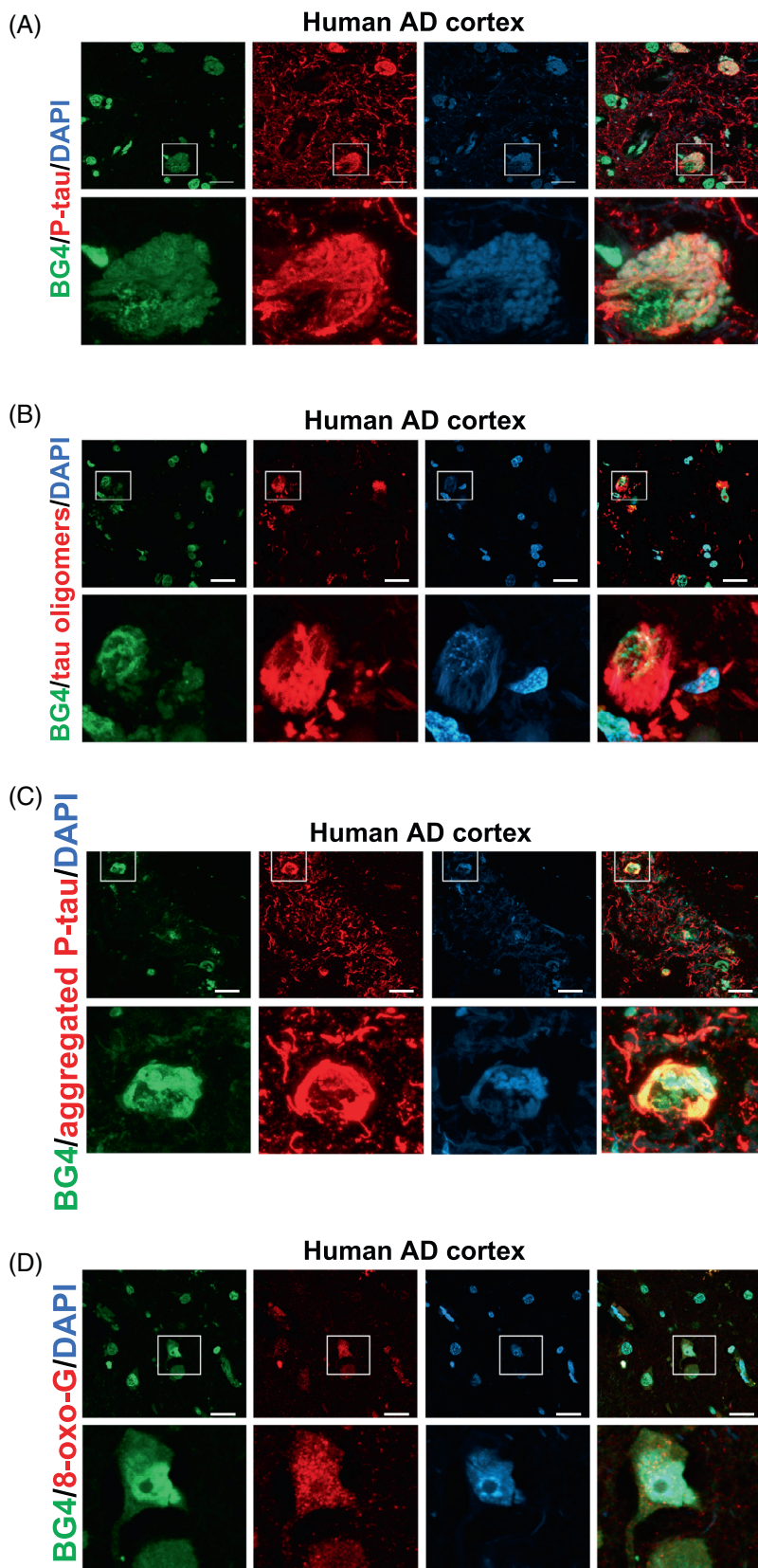


FIGURE 6 Cytoplasmic G4 DNA location correlates with pathogenic forms of tau and oxidative DNA damage in cells from human AD cerebral cortex. (A) Representative images of coronal sections from human postmortem AD brains ($n = 5$). The sections were labeled with the BG4 and anti-P-tau (AT8) antibodies. IF signals were analyzed by confocal laser-scanning microscopy (z projection). Nuclei were detected with DAPI staining. The scale bars represent 20 μm . (B) Representative images of sagittal sections from AD cortex ($n = 5$). The sections were labeled with the BG4 and anti- τ oligomers (TOC1) antibodies. IF signals were analyzed by confocal laser-scanning microscopy (z projection). Nuclei were detected with DAPI staining. The scale bars represent 20 μm . (C) Representative images of sagittal sections from AD cortex ($n = 5$). The sections were labeled with the BG4 and anti-aggregated P-tau (AT100) antibodies. IF signals were analyzed by confocal laser-scanning microscopy (z projection). Nuclei were detected with DAPI staining. The scale bars represent 20 μm . (D) Representative images of sagittal sections from AD cortex ($n = 5$). The sections were labeled with the BG4 and anti-8-oxo-G antibodies. IF signals were analyzed by confocal laser-scanning microscopy (z projection). Nuclei were detected with DAPI staining. The scale bars represent 20 μm .

production of DNA fragments. Alteration or rupture of the nuclear and/or mitochondrial envelope observed in tauopathy's models and in AD brains [62–70] could favor

the leakage of DNA fragments into the cytoplasm (Figure 7B). In addition, as guanine oxidation can modulate the formation and structuring of G4 [42], it is

tempting to hypothesize that, at early stages of tau pathology, oxidative stress could also contribute to the structuration of guanine-rich sequences in G4 (Figure 7B).

In addition to early tau pathology, amyloid plaques and small vessel disease are known to generate oxidative stress in AD brain, it would therefore be worthwhile testing their impact on G4 DNA distribution in nearby neurons.

Importantly, G4 and guanine oxidation have emerged as potent epigenetic modulators of gene expression [17, 71, 72]. It is likely that various changes in the quantity and distribution of G4-structured and oxidized DNA sequences in neuronal nuclei that we observe early during the progression of tau pathology, have severe consequences on transcription and chromatin organization.

The impact of persistent accumulation of G4-enriched DNA into the cytoplasm of neurons is a major question. Interestingly, the presence of endogenous DNA in the cytoplasm can trigger an innate immunity-type self-response, similar to that activated by viral infection [73]. Important roles of innate immunity in the development of tauopathies including AD are emerging [74–77]. We and others have recently shown interplay

between activation of the type-1 interferon response and increased tau pathology in neurons [78, 79]. However the consequences of increased DNA structuring in G4 on the activation of innate immunity in neurons is currently unknown. Interestingly, in cancer and noncancer cells, G4 binders which stabilize G4 structures can stimulate innate immunity [80]. Thus, the accumulation of G4 DNA in the cytoplasm of neurons may contribute to the progression of tau pathology through activation of innate immunity mechanisms. Still additional studies are needed to decipher potential connections between tau pathology, cytoplasmic G4 DNA, and activation of innate immunity in neurons.

Here, we focused on the impact of tau pathology on neuronal G4 DNA. Nevertheless, G4 represent only a fraction of the alternative DNA structures (H-DNA, Z-DNA, A-DNA, i-motifs, R-loops, Hairpins, Cruciform, slipped-strand DNA, etc.) to the double helix (B-DNA) [81, 82]. Therefore, the impact of tau pathology on the dynamics of secondary DNA structures other than G4s should also be considered in future.

Targeting alternative DNA structures such as G4 has been proposed as promising therapeutic strategies in cancer [11, 83, 84] and has recently emerged in the brain

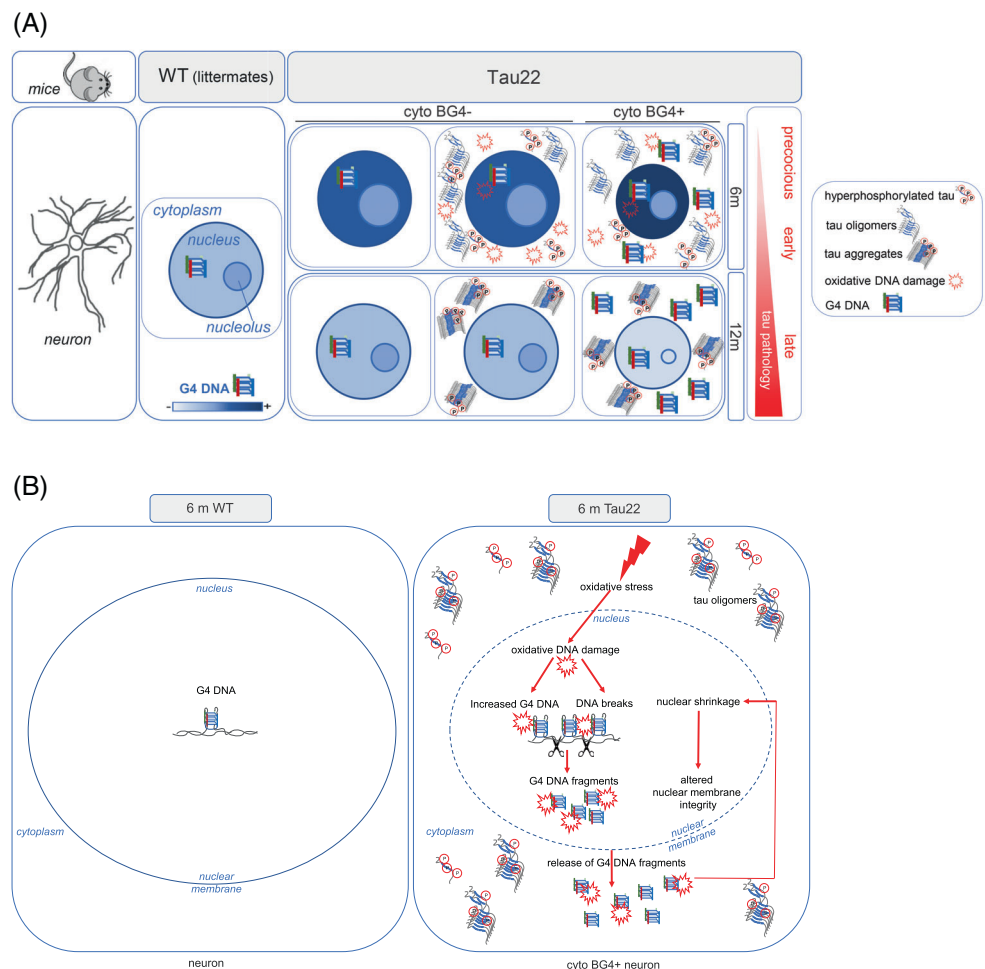


FIGURE 7 (A) Schematic summary of G4 DNA distribution combined to nuclear and nucleolar morphology in hippocampal CA1 neurons from 6 to 12 m Tau22, and WT littermate mice. (B) Hypothetical pathway leading to cytoplasmic G4 DNA accrual in neurons.

[85, 86]. Given our results and the deleterious consequences that the disruption of G4 DNA dynamics may have on cell functionality, the relevance of G4 DNA-targeting therapeutics to restrain the impact of tau pathology in neurons is worth considering.

4.3 | Impact of tau pathology on the morphology of nuclei and nucleoli in neurons

Morphological alterations of neuronal nuclei and nucleoli have been described in aging and neurodegenerative diseases including AD [7, 43, 62, 63, 65, 68, 69, 87–99]. In addition pathogenic forms of tau have been associated to disturbances of cell nuclei [70, 100].

The nucleus and nucleolus are crucial stress sensors in cells. Numerous stress can affect their shape and size, and generate a wide range of cell signals [101–103]. Here, we describe persistent compaction of neuronal nuclei starting at early stage of tau pathology, and closely associated to the presence of G4 DNA in the cytoplasm. But the potential interplay between cytoplasmic location of G4 DNA and nuclear shrinkage remains to be evaluated in neurons.

Deformations of the nucleus can favor nuclear envelope rupture leading to uncontrolled leak of nuclear components [102, 103]. Notably, nuclear shrinkage might participate to the alteration or rupture of the nuclear envelope observed in tauopathy's models and in AD brains, and favor the leak of DNA fragments into the cytoplasm of neurons [62–70] (Figure 7B). On the other hand the accumulation of G4 DNA in the cytoplasm may participate to stress induction and contribute to nuclear shrinkage in neurons, creating a vicious circle that promotes alteration of G4 DNA dynamics and nuclear morphology (Figure 7B).

In addition, we noticed opposite changes in the nucleolar morphology of neurons depending on the stage of tau pathology. We have associated nucleolar enlargement and then shrinkage to precocious and late stages of the pathology respectively. Remarkably these results recapitulate different alterations of the nucleolus size reported in neurons from AD brains, first hypertrophic nucleoli in asymptomatic AD with mild cognitive impairment and then reduced nucleolus size at late stages (Braak IV–VI) of the pathology [87–89, 91–93, 97]. Notably, Mann et al. described smaller nucleoli in tangle-bearing neurons [87]. Thus, our results suggest that contrary morphological changes of neuronal nucleoli observed in AD brains are connected to specific steps of tau pathology.

In AD brains, neurons developing tau pathology take an average of 20 years to die despite increasing dysfunction [104]. This implies that robust prosurvival mechanisms are in place to prevent cell death during all this time [39, 42, 44]. Strikingly, changes in the morphology of nucleolus have been associated with stress response

and cell survival in neurodegenerative disease including AD [96, 97].

Nucleolar expansion is an energy-consuming mechanism which quickly occurs in response to various stress in neurons, to mediate compensatory nucleolar activity and preserve neuronal viability [43, 105]. We previously reported that CA1 neurons from 6 m Tau22 mice develop transient pro-survival nuclear and mitochondrial mechanisms in response to stress, and display no overt cytotoxicity [39]. Therefore nucleolar hypertrophy appears to be an additional response to stress in neurons, to promote cell survival at precocious stage of tau pathology.

In addition, nucleolar compaction was also associated with cell survival and longevity in *C. elegans* [106]. The reduction in nucleolus size reflects a shutdown of the activity of nucleoli in response to sustained deleterious conditions to preserve cell viability in the long term. Consequently, nucleolar shrinkage that we observed in 12 m Tau22 mice may contribute to the survival of highly dysfunctional neurons bearing tau aggregates at late stage of tau pathology.

Altogether our results suggest that neurons activate different prosurvival programs to promote neuroprotection through adaptation of their nucleolar morphology in response to various stresses along the progression of tau pathology from precocious to late stages.

4.4 | Conclusion

Although highly studied in the context of cancer, the role of alternative DNA structures in neurodegenerative diseases is still in its infancy. Our results pave the way for the implication of secondary G4 DNA structures in tauopathies including AD. In addition this study highlights complex impacts of tau pathology on the mechanobiology of nuclei and nucleoli in neurons.

AUTHOR CONTRIBUTIONS

Thomas Comptdaer, Meryem Tardivel, and Marie-Christine Galas performed experiments, analyzed data and discussed results. Luc Buée discussed results and critically read the manuscript. Marie-Christine Galas designed and supervised the project and prepared the manuscript. All authors read and approved the final manuscript.

ACKNOWLEDGMENTS

We are grateful to the UAR2014/US41–PLBS (Plateformes lilloises en Biologie-Santé, Lille, France) for access to the bioimaging center platform, and to the animal facility. We are grateful to A. Bongiovanni for his assistance with confocal microscopy analyses, and to M.H. Gevaert (Laboratoire d'Histologie, Faculté de Médecine, Lille) for technical assistance. We thank Pr. Claude-Alain Maurage for his help with human brains from the Lille Neurobank (Lille, France). We

thank Pr. Vilhelm Bohr, Dr. Mansour Akbari, and Dr. Jean-Louis Mergny for fruitful discussions. We are grateful to Dr. Nicholas M. Kanaan for the generous gift of the TOC1 antibody. We express our gratitude to AD patients and their families for accepting autopsies and the use of post mortem brain material for research.

FUNDING INFORMATION

This work was supported by grants from the program Investissement d'avenir LabEx (Laboratory Excellence) DISTALZ (Development of Innovative Strategies for a Transdisciplinary approach to Alzheimer's disease). Our laboratories are also supported by LICEND (Lille Centre of Excellence for Neurodegenerative Disorders), CNRS (Centre National de la Recherche Scientifique), Inserm (Institut National de la Santé et de la Recherche Médicale), Métropole Européenne de Lille, University of Lille and Fonds européen de développement régional (FEDER). M-C.G was also supported by INSTALZ, an EU Joint Programme–Neurodegenerative Disease Research (JPND) project. The INSTALZ project is supported through the following funding organisations under the aegis of JPND—“<http://www.jpnd.eu>” (Belgium, Research Foundation Flanders; Denmark, Innovation Fund Denmark; France, Agence Nationale de la Recherche; Sweden, Swedish Research Council; UK, Medical Research Council). The project has received funding from the European Union's Horizon 2020 research and innovation programme.

CONFLICT OF INTEREST STATEMENT

The authors declare that they have no conflict of interest.

DATA AVAILABILITY STATEMENT

No data was used for the research described in the article.

ETHICS STATEMENT

The animals were maintained in compliance with institutional protocols (Comité d'éthique en expérimentation animale du Nord Pas-de-Calais, no. 0508003). All of the animal experiments were performed in compliance with and following the approval of the local Animal Ethical Committee (agreement #12787–2, 015, 101, 320, 441, 671 v9n from CEEA75, Lille, France), standards for the care and use of laboratory animals, and the French and European Community rules.

ORCID

Marie-Christine Galas  <https://orcid.org/0000-0002-3766-7103>

REFERENCES

- Avila J, Jiménez JS, Sayas CL, Bolós M, Zabala JC, Rivas G, et al. Tau Structures. *Front Aging Neurosci.* 2016;8(8):262. <https://doi.org/10.3389/fnagi.2016.00262>
- Kampers T, Friedhoff P, Biernat J, Mandelkow EM, Mandelkow E. RNA stimulates aggregation of microtubule-associated protein tau into Alzheimer-like paired helical filaments. *FEBS Lett.* 1996;399(3):344–9. [https://doi.org/10.1016/s0014-5793\(96\)01386-5](https://doi.org/10.1016/s0014-5793(96)01386-5)
- Dinkel PD, Holden MR, Matin N, Margittai M. RNA binds to tau fibrils and sustains template-assisted growth. *Biochemistry.* 2015;54(30):4731–40. <https://doi.org/10.1021/acs.biochem.5b00453>
- Ambadipudi S, Biernat J, Riedel D, Mandelkow E, Zweckstetter M. Liquid-liquid phase separation of the microtubule-binding repeats of the Alzheimer-related protein tau. *Nat Commun.* 2017;8(1):275. <https://doi.org/10.1038/s41467-017-00480-0>
- Ginsberg SD, Crino PB, Lee VM, Eberwine JH, Trojanowski JQ. Sequestration of RNA in Alzheimer's disease neurofibrillary tangles and senile plaques. *Ann Neurol.* 1997;41(2):200–9. <https://doi.org/10.1002/ana.410410211>
- Lester E, Ooi FK, Bakkar N, Ayers J, Woerman AL, Wheeler J, et al. Tau aggregates are RNA-protein assemblies that mislocalize multiple nuclear speckle components. *Neuron.* 2021;109(10):1675–1691.e9. <https://doi.org/10.1016/j.neuron.2021.03.026>
- Jiang L, Lin W, Zhang C, Ash PEA, Verma M, Kwan J, et al. Interaction of tau with HNRNPA2B1 and N⁶-methyladenosine RNA mediates the progression of tauopathy. *Mol Cell.* 2021;81(20):4209–4227.e12. <https://doi.org/10.1016/j.molcel.2021.07.038>
- McMillan PJ, Benbow SJ, Uhrich R, Saxton A, Baum M, Strovast T, et al. Tau-RNA complexes inhibit microtubule polymerization and drive disease-relevant conformation change. *Brain.* 2023;146(8):3206–20. <https://doi.org/10.1093/brain/awad032>
- Zwierzchowski-Zarate AN, Mendoza-Oliva A, Kashmer OM, Collazo-Lopez JE, White CL 3rd, Diamond MI. RNA induces unique tau strains and stabilizes Alzheimer's disease seeds. *J Biol Chem.* 2022;298(8):102132. <https://doi.org/10.1016/j.jbc.2022.102132>
- Shmookler Reis RJ, Atluri R, Balasubramaniam M, Johnson J, Ganne A, Ayyadevara S. "Protein aggregates" contain RNA and DNA, entrapped by misfolded proteins but largely rescued by slowing translational elongation. *Aging Cell.* 2021;20(5):e13326. <https://doi.org/10.1111/accel.13326>
- Varshney D, Spiegel J, Zyner K, Tannahill D, Balasubramanian S. The regulation and functions of DNA and RNA G-quadruplexes. *Nat Rev Mol Cell Biol.* 2020;21(8):459–74. <https://doi.org/10.1038/s41580-020-0236-x>
- Spiegel J, Adhikari S, Balasubramanian S. The structure and function of DNA G-quadruplexes. *Trends Chem.* 2020;2(2):123–36. <https://doi.org/10.1016/j.trechm.2019.07.002>
- Johnson FB. Fundamentals of G-quadruplex biology. *Annu Rep Med Chem.* 2020;54:3–44. <https://doi.org/10.1016/bs.armac.2020.06.004>
- Moruno-Manchon JF, Koellhoffer EC, Gopakumar J, Hambarde S, Kim N, McCullough LD, et al. The G-quadruplex DNA stabilizing drug pyridostatin promotes DNA damage and downregulates transcription of Brca1 in neurons. *Aging (Albany NY).* 2017;9(9):1957–70. <https://doi.org/10.18632/aging.101282>
- Reina C, Cavalieri V. Epigenetic modulation of chromatin states and gene expression by G-quadruplex structures. *Int J Mol Sci.* 2020;21(11):4172. <https://doi.org/10.3390/ijms21114172>
- Pavlova AV, Kubareva EA, Monakhova MV, Zvereva MI, Dolinnaya NG. Impact of G-quadruplexes on the regulation of genome integrity, DNA damage and repair. *Biomolecules.* 2021;11(9):1284. <https://doi.org/10.3390/biom11091284>
- Robinson J, Raguseo F, Nuccio SP, Liano D, Di Antonio M. DNA G-quadruplex structures: more than simple roadblocks to transcription? *Nucleic Acids Res.* 2021;49(15):8419–31. <https://doi.org/10.1093/nar/gkab609>
- Yuan J, He X, Wang Y. G-quadruplex DNA contributes to RNA polymerase II-mediated 3D chromatin architecture. *Nucleic Acids Res.* 2023;51(16):8434–46. <https://doi.org/10.1093/nar/gkad588>

19. Maizels N. G4-associated human diseases. *EMBO Rep.* 2015; 16(8):910–22. <https://doi.org/10.15252/embr.201540607>
20. François M, Leifert WR, Hecker J, Faunt J, Fenech MF. Guanine-quadruplexes are increased in mild cognitive impairment and correlate with cognitive function and chromosomal DNA damage. *DNA Repair (Amst).* 2016;46:29–36. <https://doi.org/10.1016/j.dnarep.2016.08.001>
21. Asamitsu S, Takeuchi M, Ikenoshita S, Imai Y, Kashiwagi H, Shioda N. Perspectives for applying G-quadruplex structures in neurobiology and neuropharmacology. *Int J Mol Sci.* 2019;20(12): 2884. <https://doi.org/10.3390/ijms20122884>
22. Begeman A, Son A, Litberg TJ, Wroblewski TH, Gehring T, Huizar Cabral V, et al. G-Quadruplexes act as sequence-dependent protein chaperones. *EMBO Rep.* 2020;21(10):e49735. [10.15252/embr.201949735](https://doi.org/10.15252/embr.201949735).
23. Hanna R, Flamier A, Barabino A, Bernier G. G-quadruplexes originating from evolutionary conserved L1 elements interfere with neuronal gene expression in Alzheimer's disease. *Nat Commun.* 2021;12(1):1828. <https://doi.org/10.1038/s41467-021-22129-9>.
24. Wang E, Thombre R, Shah Y, Latanich R, Wang J. G-quadruplexes as pathogenic drivers in neurodegenerative disorders. *Nucleic Acids Res.* 2021;49(9):4816–30. <https://doi.org/10.1093/nar/gkab164>
25. Guzman BB, Son A, Litberg TJ, Huang Z, Dominguez D, Horowitz S. Emerging roles for G-quadruplexes in proteostasis. *FEBS J.* 2023;290(19):4614–25. <https://doi.org/10.1111/febs.16608>
26. Son A, Huizar Cabral V, Huang Z, Litberg TJ, Horowitz S. G-quadruplexes rescuing protein folding. *Proc Natl Acad Sci U S A.* 2023;120(20):e2216308120. <https://doi.org/10.1073/pnas.2216308120>
27. Vijay Kumar MJ, Morales R, Tsvetkov AS. G-quadruplexes and associated proteins in aging and Alzheimer's disease. *Front Aging.* 2023;1(4):1164057. <https://doi.org/10.3389/fragi.2023.1164057>
28. Litberg TJ, Sannapureddi RKR, Huang Z, Son A, Sathyamoorthy B, Horowitz S. Why are G-quadruplexes good at preventing protein aggregation? *RNA Biol.* 2023;20(1):495–509. <https://doi.org/10.1080/15476286.2023.2228572>
29. Lorenzatti A, Piga EJ, Gismondi M, Binolfi A, Margarit E, Calcaterra NB, et al. Genetic variations in G-quadruplex forming sequences affect the transcription of human disease-related genes. *Nucleic Acids Res.* 2023;51(22):12124–39. <https://doi.org/10.1093/nar/gkad948>
30. Kallweit L, Hamlett ED, Saternos H, Gilmore A, Granholm AC, Horowitz S. A new role for RNA G-quadruplexes in aging and Alzheimer's disease. *bioRxiv.* 2023. <https://doi.org/10.1101/2023.10.02.560545>
31. Schindowski K, Bretteville A, Leroy K, Begard S, Brion JP, Hamdane M, et al. Alzheimer's disease-like tau neuropathology leads to memory deficits and loss of functional synapses in a novel mutated tau transgenic mouse without any motor deficits. *Am J Pathol.* 2006;169:599–616. <https://doi.org/10.2353/ajpath.2006.060002>
32. van der Jeugd A, Vermaercke B, Derisbourg M, Lo AC, Hamdane M, Blum D, et al. Progressive age-related cognitive decline in tau mice. *J Alzheimers Dis.* 2013;37(4):777–88. <https://doi.org/10.3233/JAD-130110>
33. Laurent C, Burnouf S, Ferry B, Batalha VL, Coelho JE, Baqi Y, et al. A2A adenosine receptor deletion is protective in a mouse model of tauopathy. *Mol Psychiatry.* 2016;21(1):97–107. <https://doi.org/10.1038/mp.2014.151>
34. Patterson KR, Remmers C, Fu Y, Brooker S, Kanaan NM, Vana L, et al. Characterization of prefibrillar tau oligomers in vitro and in Alzheimer disease. *J Biol Chem.* 2011;286(26): 23063–76. <https://doi.org/10.1074/jbc.M111.237974>
35. Zheng-Fischhöfer Q, Biernat J, Mandelkow EM, Illenberger S, Godemann R, Mandelkow E. Sequential phosphorylation of tau by glycogen synthase kinase-3beta and protein kinase a at Thr212 and Ser214 generates the Alzheimer-specific epitope of antibody AT100 and requires a paired-helical-filament-like conformation. *Eur J Biochem.* 1998;252(3):542–52. <https://doi.org/10.1046/j.1432-1327.1998.2520542.x>
36. Biffi G, Tannahill D, McCafferty J, Balasubramanian S. Quantitative visualization of DNA G-quadruplex structures in human cells. *Nat Chem.* 2013;5(3):182–6. <https://doi.org/10.1038/nchem.1548>
37. Javadekar SM, Nilavar NM, Paranjape A, Das K, Raghavan SC. Characterization of G-quadruplex antibody reveals differential specificity for G4 DNA forms. *DNA Res.* 2020;27(5):dsaa024. <https://doi.org/10.1093/dnares/dsaa024>
38. Benhelli-Mokrani H, Mansuroglu Z, Chauderlier A, Albaud B, Gentien D, Sommer S, et al. Genome-wide identification of genic and intergenic neuronal DNA regions bound by tau protein under physiological and stress conditions. *Nucleic Acids Res.* 2018; 46(21):11405–22. <https://doi.org/10.1093/nar/gky929>
39. Zheng J, Akbari M, Schirmer C, Reynaert ML, Loyens A, Lefebvre B, et al. Hippocampal tau oligomerization early in tau pathology coincides with a transient alteration of mitochondrial homeostasis and DNA repair in a mouse model of tauopathy. *Acta Neuropathol Commun.* 2020;8(1):25. <https://doi.org/10.1186/s40478-020-00896-8>
40. Ward SM, Himmelstein DS, Lancia JK, Fu Y, Patterson KR, Binder LI. TOC1: characterization of a selective oligomeric tau antibody. *J Alzheimers Dis.* 2013;37:593–602. <https://doi.org/10.3233/JAD-131235>
41. Bielskute S, Plavec J, Podbevšek P. Oxidative lesions modulate G-quadruplex stability and structure in the human BCL2 promoter. *Nucleic Acids Res.* 2021;49(4):2346–56. <https://doi.org/10.1093/nar/gkab057>
42. Wu S, Jiang L, Lei L, Fu C, Huang J, Hu Y, et al. Crosstalk between G-quadruplex and ROS. *Cell Death Dis.* 2023;14(1):37. <https://doi.org/10.1038/s41419-023-05562-0>
43. Buchwalter A, Hetzer MW. Nucleolar expansion and elevated protein translation in premature aging. *Nat Commun.* 2017;8(1): 328. <https://doi.org/10.1038/s41467-017-00322-z>
44. Denechaud M, Geurs S, Comptdaer T, Bégard S, Garcia-Núñez A, Pechereau LA, et al. Tau promotes oxidative stress-associated cycling neurons in S phase as a pro-survival mechanism: possible implication for Alzheimer's disease. *Prog Neurobiol.* 2023;223:102386. <https://doi.org/10.1016/j.pneurobio.2022.102386>
45. Asamitsu S, Imai Y, Yabuki Y, Ikenoshita S, Takeuchi M, Kashiwagi H, et al. Identification and immunohistochemical characterization of G-quadruplexes in mouse brain. *Biochem Biophys Res Commun.* 2020;531(1):67–74. <https://doi.org/10.1016/j.bbrc.2020.01.145>
46. Smirnov E, Cmarko D, Mazel T, Hornáček M, Raška I. Nucleolar DNA: the host and the guests. *Histochem Cell Biol.* 2016; 145(4):359–72. <https://doi.org/10.1007/s00418-016-1407-x>
47. Hanakahi LA, Sun H, Maizels N. High affinity interactions of nucleolin with G-G-paired rDNA. *J Biol Chem.* 1999;274(22): 15908–12. <https://doi.org/10.1074/jbc.274.22.15908>
48. Hershman SG, Chen Q, Lee JY, Kozak ML, Yue P, Wang LS, et al. Genomic distribution and functional analyses of potential G-quadruplex-forming sequences in *Saccharomyces cerevisiae*. *Nucleic Acids Res.* 2008;36(1):144–56. <https://doi.org/10.1093/nar/gkm986>
49. Datta A, Pollock KJ, Kormuth KA, Brosh RM Jr. G-quadruplex assembly by ribosomal DNA: emerging roles in disease pathogenesis and cancer biology. *Cytogenet Genome Res.* 2021;161(6–7): 285–96. <https://doi.org/10.1159/000516394>
50. Hoffmann RF, Moshkin YM, Mouton S, Grzeschik NA, Kalicharan RD, Kuipers J, et al. Guanine quadruplex structures localize to heterochromatin. *Nucleic Acids Res.* 2016;44(1):152–63. <https://doi.org/10.1093/nar/gkv900>
51. Hänsel-Hertsch R, Beraldi D, Lensing SV, Marsico G, Zyner K, Parry A, et al. G-quadruplex structures mark human regulatory chromatin. *Nat Genet.* 2016;48(10):1267–72. <https://doi.org/10.1038/ng.3662>

52. Ray S, Tillo D, Boer RE, Assad N, Barshai M, Wu G, et al. Custom DNA microarrays reveal diverse binding preferences of proteins and small molecules to thousands of G-quadruplexes. *ACS Chem Biol.* 2020;15(4):925–35. <https://doi.org/10.1021/acscchembio.9b00934>
53. Summers PA, Lewis BW, Gonzalez-Garcia J, Porreca RM, Lim AHM, Cadinu P, et al. Visualising G-quadruplex DNA dynamics in live cells by fluorescence lifetime imaging microscopy. *Nat Commun.* 2021;12(1):162. <https://doi.org/10.1038/s41467-020-20414-7>
54. Miller KN, Victorelli SG, Salmonowicz H, Dasgupta N, Liu T, Passos JF, et al. Cytoplasmic DNA: sources, sensing, and role in aging and disease. *Cell.* 2021;184(22):5506–26. <https://doi.org/10.1016/j.cell.2021.09.034>
55. Kosik KS, Han S. Tau Condensates. *Adv Exp Med Biol.* 2019;1184:327–39. https://doi.org/10.1007/978-981-32-9358-8_24
56. Wegmann S. Liquid-liquid phase separation of tau protein in neurobiology and pathology. *Adv Exp Med Biol.* 2019;1184:341–57. https://doi.org/10.1007/978-981-32-9358-8_25
57. Rai SK, Savastano A, Singh P, Mukhopadhyay S, Zweckstetter M. Liquid-liquid phase separation of tau: from molecular biophysics to physiology and disease. *Protein Sci.* 2021;30(7):1294–314. <https://doi.org/10.1002/pro.4093>
58. Najafi S, Lin Y, Longhini AP, Zhang X, Delaney KT, Kosik KS, et al. Liquid-liquid phase separation of tau by self and complex coacervation. *Protein Sci.* 2021;30(7):1393–407. <https://doi.org/10.1002/pro.4101>
59. Ainani H, Bouchmaa N, Ben Mrid R, El Fatimy R. Liquid-liquid phase separation of protein tau: An emerging process in Alzheimer's disease pathogenesis. *Neurobiol Dis.* 2023;178:106011. <https://doi.org/10.1016/j.nbd.2023.106011>
60. Gao Z, Yuan J, He X, Wang H, Wang Y. Phase separation modulates the formation and stabilities of DNA guanine quadruplex. *JACS Au.* 2023;3(6):1650–7. <https://doi.org/10.1021/jacsau.3c00106>
61. Byrd AK, Zybaïlov BL, Maddukuri L, Gao J, Marecki JC, Jaiswal M, et al. Evidence that G-quadruplex DNA accumulates in the cytoplasm and participates in stress granule assembly in response to oxidative stress. *J Biol Chem.* 2016;291(34):18041–57. <https://doi.org/10.1074/jbc.M116.718478>
62. Frost B, Bardai FH, Feany MB. Lamin dysfunction mediates neurodegeneration in tauopathies. *Curr Biol.* 2016;26(1):129–36. <https://doi.org/10.1016/j.cub.2015.11.039>
63. Eftekhazadeh B, Daigle JG, Kapinos LE, Coyne A, Schiantarelli J, Carlomagno Y, et al. Tau protein disrupts nucleocytoplasmic transport in Alzheimer's disease. *Neuron.* 2018;99(5):925–940.e7. <https://doi.org/10.1016/j.neuron.2018.07.039>
64. Cornelison GL, Levy SA, Jenson T, Frost B. Tau-induced nuclear envelope invagination causes a toxic accumulation of mRNA in drosophila. *Aging Cell.* 2019;18(1):e12847. <https://doi.org/10.1111/acer.12847>
65. Paonessa F, Evans LD, Solanki R, Larrieu D, Wray S, Hardy J, et al. Microtubules deform the nuclear membrane and disrupt nucleocytoplasmic transport in tau-mediated frontotemporal dementia. *Cell Rep.* 2019;26(3):582–593.e5. <https://doi.org/10.1016/j.celrep.2018.12.085>
66. Montalbano M, McAllen S, Puangmalai N, Sengupta U, Bhatt N, Johnson OD, et al. RNA-binding proteins Musashi and tau soluble aggregates initiate nuclear dysfunction. *Nat Commun.* 2020;11(1):4305. <https://doi.org/10.1038/s41467-020-18022-6>
67. Diez L, Wegmann S. Nuclear transport deficits in tau-related neurodegenerative diseases. *Front Neurol.* 2020;25(11):1056. <https://doi.org/10.3389/fneur.2020.01056>
68. Montalbano M, Majmundar L, Sengupta U, Fung L, Kaye R. Pathological tau signatures and nuclear alterations in neurons, astrocytes and microglia in Alzheimer's disease, progressive supranuclear palsy, and dementia with Lewy bodies. *Brain Pathol.* 2023;33(1):e13112. <https://doi.org/10.1111/bpa.13112>
69. Prissette M, Fury W, Koss M, Racioppi C, Fedorova D, Dragileva E, et al. Disruption of nuclear envelope integrity as a possible initiating event in tauopathies. *Cell Rep.* 2022;40(8):111249. <https://doi.org/10.1016/j.celrep.2022.111249>
70. Sohn C, Ma J, Ray WJ, Frost B. Pathogenic tau decreases nuclear tension in cultured neurons. *Front Aging.* 2023;23(4):1058968. <https://doi.org/10.3389/fragi.2023.1058968>
71. Varizhuk A, Isaakova E, Pozmogova G. DNA G-quadruplexes (G4s) modulate epigenetic (Re)programming and chromatin remodeling: transient genomic G4s assist in the establishment and maintenance of epigenetic Marks, while persistent G4s may erase epigenetic Marks. *Bioessays.* 2019;41(9):e1900091. <https://doi.org/10.1002/bies.201900091>
72. Gorini F, Ambrosio S, Lania L, Majello B, Amente S. The intertwined role of 8-oxodG and G4 in transcription regulation. *Int J Mol Sci.* 2023;24(3):2031. <https://doi.org/10.3390/ijms24032031>
73. Akbari M, Shanley DP, Bohr VA, Rasmussen LJ. Cytosolic self-DNA-A potential source of chronic inflammation in aging. *Cells.* 2021;10(12):3544. <https://doi.org/10.3390/cells10123544>
74. Roy ER, Wang B, Wan YW, Chiu G, Cole A, Yin Z, et al. Type I interferon response drives neuroinflammation and synapse loss in Alzheimer disease. *J Clin Invest.* 2020;130(4):1912–30. <https://doi.org/10.1172/JCI133737>
75. Tamburini B, Badami GD, La Manna MP, Shekarkar Azgomi M, Caccamo N, Dieli F. Emerging roles of cells and molecules of innate immunity in Alzheimer's disease. *Int J Mol Sci.* 2023;24(15):11922. <https://doi.org/10.3390/ijms241511922>
76. Langworth-Green C, Patel S, Jaunmuktane Z, Jabbari E, Morris H, Thom M, et al. Chronic effects of inflammation on tauopathies. *Lancet Neurol.* 2023;22(5):430–42. [https://doi.org/10.1016/S1474-4422\(23\)00038-8](https://doi.org/10.1016/S1474-4422(23)00038-8)
77. Johnson AM, Lukens JR. The innate immune response in tauopathies. *Eur J Immunol.* 2023;53(6):e2250266. <https://doi.org/10.1002/eji.202250266>
78. Manet C, Mansuroglu Z, Conquet L, Bortolin V, Comptdaer T, Segrt H, et al. Zika virus infection of mature neurons from immunocompetent mice generates a disease-associated microglia and a tauopathy-like phenotype in link with a delayed interferon beta response. *J Neuroinflammation.* 2022;19(1):307. <https://doi.org/10.1186/s12974-022-02668-8>
79. Sanford SAI, Miller LVC, Vaysburd M, Keeling S, Tuck BJ, Clark J, et al. The type-I interferon response potentiates seeded tau aggregation and exacerbates tau pathology. *Alzheimers Dement.* 2024;20(2):1025. <https://doi.org/10.1002/alz.13493>
80. Miglietta G, Marinello J, Russo M, Capranico G. Ligands stimulating antitumour immunity as the next G-quadruplex challenge. *Mol Cancer.* 2022;21(1):180. <https://doi.org/10.1186/s12943-022-01649-y>
81. Duardo RC, Guerra F, Pepe S, Capranico G. Non-B DNA structures as a booster of genome instability. *Biochimie.* 2023;214:176–92. <https://doi.org/10.1016/j.biochi.2023.07.002>
82. Matos-Rodrigues G, Hisey JA, Nussenzweig A, Mirkin SM. Detection of alternative DNA structures and its implications for human disease. *Mol Cell.* 2023;83(20):3622–41. <https://doi.org/10.1016/j.molcel.2023.08.018>
83. Nakanishi C, Seimiya H. G-quadruplex in cancer biology and drug discovery. *Biochem Biophys Res Commun.* 2020;531(1):45–50. <https://doi.org/10.1016/j.bbrc.2020.03.178>
84. Carvalho J, Mergny JL, Salgado GF, Queiroz JA, Cruz C. G-quadruplex, friend or foe: the role of the G-quartet in anticancer strategies. *Trends Mol Med.* 2020;26(9):848–61. <https://doi.org/10.1016/j.molmed.2020.05.002>
85. Shioda N, Yabuki Y, Yamaguchi K, Onozato M, Li Y, Kurosawa K, et al. Targeting G-quadruplex DNA as cognitive function therapy for ATR-X syndrome. *Nat Med.* 2018;24(6):802–13. <https://doi.org/10.1038/s41591-018-0018-6>
86. Asamitsu S, Yabuki Y, Ikenoshita S, Wada T, Shioda N. Pharmacological prospects of G-quadruplexes for neurological diseases

- using porphyrins. *Biochem Biophys Res Commun.* 2020;531(1):51–5. <https://doi.org/10.1016/j.bbrc.2020.01.054>
87. Mann DM, Neary D, Yates PO, Lincoln J, Snowden JS, Stanworth P. Alterations in protein synthetic capability of nerve cells in Alzheimer's disease. *J Neurol Neurosurg Psychiatry.* 1981;44(2):97–102. <https://doi.org/10.1136/jnnp.44.2.97>
 88. Tagliavini F, Pilleri G. Basal nucleus of Meynert. a neuropathological study in Alzheimer's disease, simple senile dementia, Pick's disease and Huntington's chorea. *J Neurol Sci.* 1983;62(1–3):243–60. [https://doi.org/10.1016/0022-510x\(83\)90203-4](https://doi.org/10.1016/0022-510x(83)90203-4)
 89. Mann DM, Marcyniuk B, Yates PO, Neary D, Snowden JS. The progression of the pathological changes of Alzheimer's disease in frontal and temporal neocortex examined both at biopsy and at autopsy. *Neuropathol Appl Neurobiol.* 1988;14(3):177–95. <https://doi.org/10.1111/j.1365-2990.1988.tb00880.x>
 90. Riudavets MA, Iacono D, Resnick SM, O'Brien R, Zonderman AB, Martin LJ, et al. Resistance to Alzheimer's pathology is associated with nuclear hypertrophy in neurons. *Neurobiol Aging.* 2007;28(10):1484–92. <https://doi.org/10.1016/j.neurobiolaging.2007.05.005>
 91. Iacono D, O'Brien R, Resnick SM, Zonderman AB, Pletnikova O, Rudow G, et al. Neuronal hypertrophy in asymptomatic Alzheimer disease. *J Neuropathol Exp Neurol.* 2008;67(6):578–89. <https://doi.org/10.1097/NEN.0b013e3181772794>
 92. Iacono D, Markesbery WR, Gross M, Pletnikova O, Rudow G, Zandi P, et al. The nun study: clinically silent AD, neuronal hypertrophy, and linguistic skills in early life. *Neurology.* 2009;73(9):665–73. <https://doi.org/10.1212/WNL.0b013e3181b01077>
 93. Hetman M, Pietrzak M. Emerging roles of the neuronal nucleolus. *Trends Neurosci.* 2012;35(5):305–14. <https://doi.org/10.1016/j.tins.2012.01.002>
 94. Nyhus C, Pihl M, Hyttel P, Hall VJ. Evidence for nucleolar dysfunction in Alzheimer's disease. *Rev Neurosci.* 2019;30(7):685–700. <https://doi.org/10.1515/revneuro-2018-0104>
 95. Ishunina TA, Bogolepova IN, Swaab DF. Increased neuronal nuclear and perikaryal size in the medial mamillary nucleus of vascular dementia and Alzheimer's disease patients: relation to nuclear estrogen receptor α . *Dement Geriatr Cogn Disord.* 2019;47(4–6):274–80. <https://doi.org/10.1159/000500244>
 96. Aladesuyi Arogundade O, Nguyen S, Leung R, Wainio D, Rodriguez M, Ravits J. Nucleolar stress in C9orf72 and sporadic ALS spinal motor neurons precedes TDP-43 mislocalization. *Acta Neuropathol Commun.* 2021;9(1):26. <https://doi.org/10.1186/s40478-021-01125-6>
 97. Iatrou A, Clark EM, Wang Y. Nuclear dynamics and stress responses in Alzheimer's disease. *Mol Neurodegeneration.* 2021;16(1):65. <https://doi.org/10.1186/s13024-021-00489-6>
 98. Pathak RU, Soujanya M, Mishra RK. Deterioration of nuclear morphology and architecture: a hallmark of senescence and aging. *Ageing Res Rev.* 2021;67:101264. <https://doi.org/10.1016/j.arr.2021.101264>
 99. Dickson JR, Frosch MP, Hyman BT. Altered localization of nucleoporin 98 in primary tauopathies. *Brain Commun.* 2022;5(1):fcac334. <https://doi.org/10.1093/braincomms/fcac334>
 100. Sun X, Eastman G, Shi Y, Saibaba S, Oliveira AK, Lukens JR, et al. Structural and functional damage to neuronal nuclei caused by extracellular tau oligomers. *Alzheimers Dement.* 2023;20:1656–70. <https://doi.org/10.1002/alz.13535>
 101. Jamieson SM, Liu JJ, Connor B, Draganow M, McKeage MJ. Nucleolar enlargement, nuclear eccentricity and altered cell body immunostaining characteristics of large-sized sensory neurons following treatment of rats with paclitaxel. *Neurotoxicology.* 2007;28(6):1092–8. <https://doi.org/10.1016/j.neuro.2007.04.009>
 102. Nader GPF, Williard A, Piel M. Nuclear deformations, from signaling to perturbation and damage. *Curr Opin Cell Biol.* 2021;72:137–45. <https://doi.org/10.1016/j.ceb.2021.07.008>
 103. Kalukula Y, Stephens AD, Lammerding J, Gabriele S. Mechanics and functional consequences of nuclear deformations. *Nat Rev Mol Cell Biol.* 2022;23(9):583–602. <https://doi.org/10.1038/s41580-022-00480-z>
 104. Morsch R, Simon W, Coleman PD. Neurons may live for decades with neurofibrillary tangles. *J Neuropathol Exp Neurol.* 1999;58(2):188–97. <https://doi.org/10.1097/00005072-199902000-00008>
 105. Kubben N, Misteli T. Shared molecular and cellular mechanisms of premature ageing and ageing-associated diseases. *Nat Rev Mol Cell Biol.* 2017;18(10):595–609. <https://doi.org/10.1038/nrm.2017.68>
 106. Tiku V, Jain C, Raz Y, Nakamura S, Heestand B, Liu W, et al. Small nucleoli are a cellular hallmark of longevity. *Nat Commun.* 2017;30(8):16083. <https://doi.org/10.1038/ncomms16083>

SUPPORTING INFORMATION

Additional supporting information can be found online in the Supporting Information section at the end of this article.

How to cite this article: Comptdaer T, Tardivel M, Schirmer C, Buée L, Galas M-C. Cell redistribution of G quadruplex-structured DNA is associated with morphological changes of nuclei and nucleoli in neurons during tau pathology progression. *Brain Pathology.* 2024. e13262. <https://doi.org/10.1111/bpa.13262>